UNIVERSITÀ DEGLI STUDI DI ROMA TOR VERGATA

DEPARTMENT OF ENTERPRISE ENGINEERING "MARIO LUCERTINI"
PHD PROGRAM IN DESIGN, MANUFACTURING AND OPERATIONS ENGINEERING

DOCTORAL THESIS IN REVERSE ENGINEERING

AN INVESTIGATION ON DIGITAL TWIN METHODOLOGIES FOR THE ITER PROJECT

Candidate:

Edoardo Pompa

Advisor:

Prof. Marco E. Biancolini

Co-Advisors:

Dr. Gabriele D'Amico
C.E.T. Alessandro Lo Bue

Cycle XXXIV a.a. 2018/2019

Quale che sia la posizione nella quale ci si confronta, qualche cosa

rimane di noi negli altri e degli altri in noi.

Acknowledgements

Forewords

The activities of this PhD thesis are oriented around the ITER project. The nuclear power plant being built in France, is not only the key experiment for the energy transition, but it is the incubator for cutting edge technologies and a great engine for the development of world industry.

I have been introduced to the project by professor Marco Biancolini. I had the chance to join the F4E organization, the European Domestic Agency undertaking ITER, in 2017 as a trainee in the Analysis and Codes group. At the end of this first experience, culminating in the publication of my master thesis on fracture mechanics, I have been offered to join the Metrology group, and to renovate my interest in the research field through this PhD.

During these years in the Metrology group, I had the opportunity to visit several industrial realities revolving around two of the main European programs for ITER, the Vacuum Vessel (VV) and Toroidal Field coils (TF). While learning the basics of the measurement process, from Geometric Dimensioning & Tolerancing to Uncertainty estimation, I witnessed how metrology and reverse engineering are implemented in the production. I experienced how these processes integrate in the manufacturing, drive the decision making and affect the production plan.

From this privileged standpoint and with the support of the F4E Metrology group, I started my investigation on the state of the art of Digital Twins model and Industry 4.0. Through this study I discovered which are the technologies and standards deployed up today. Skin Surface models and Geospelling are the two main methodologies that inspired the main exercises of reconstruction of as-built CAD geometries and association of measured data to the nominal models which have been reported in this thesis. Such activities presented a basis for the development of a virtual model of the component in production, which serves as a journal of deviations occurred during manufacturing. After commissioning, the same model can monitor

the component actual performances, and it can offer a synthesis between the several stages of the component lifecycle.

Although far from being a conclusive work, the insight proposed by these exercises has been the basis for other works on the topic, such as the Virtual Fitting test presented in the corresponding paragraph on the alignment of measurement data to the nominal model. Furthermore, finding their application on the production of ITER components, the outcome of the tests has been used already for the improvement of critical manufacturing steps.

Abstract

The world current energy demand is of 12 TW and due to the world population exponential growing it is expected to increase by 37% by 2040 (according to the IEA 2014 Executive Summary).

Today 87% of the global energy consumption is based on fossil fuels, with oil 33% and coal 30% as the primary energy resources, followed by hydropower (7%) and nuclear (4%) energy. Renewable energy has only a small fraction in the energy consumption (2%).The need to change this dependence is critical for the reduction of greenhouse gas emissions and the global warming.

Fusion energy is a valuable alternative to today commercial energy sources. Once harnessed it has the potential to be nearly unlimited, safe, free from greenhouse emission and long-lived radioactive by-products.

The principle behind fusion energy is the same of the stars: elements are fused together into heavier ones with an associated energy release. While in the sun the nuclear reaction is obtained with the fusion of hydrogen into helium driven by gravity, to achieve the same results on earth a different approach is required. The most efficient one in terms of energy produced versus temperature required is setting the reaction to be between deuterium and tritium, two hydrogen isotopes.

The tokamak is one of the solutions designed to make this reaction possible and to harness the energy of fusion. Inside the tokamak, the energy produced is absorbed as heat in the walls of the vessel, then to be converted in electrical energy by means of classical loops (steam generator, turbines) as a conventional power plant. A number of tokamaks are nowadays available as experimental reactors (i.e. the JET machine in the U.K) demonstrating the possibility or reproduce the fusion reaction in a controlled way, however all these machines aren't able to generate more energy than the one necessary to make the fusion reaction happen.

ITER ("The Way" in Latin) is one of the most ambitious energy projects in the world today. In Cadarache, southern France, the ITER members (China, the European Union, India, Japan, Korea, Russia and the United States) are collaborating to build the world's largest tokamak to prove the feasibility of fusion. ITER will be the first fusion device to produce net energy, with an estimated output of 500 MW of fusion power from 50 MW of input heating power. It will maintain fusion for long periods of time and will test the integrated technologies, materials, and physics regimes necessary for the commercial production of fusion-based electricity.

ITER will achieve the fusion reaction of deuterium and tritium using strong magnetic fields (around 12 T) to confine the high temperature plasma (150M C°, ten times the temperature occurring for the hydrogen reaction in the sun) during pulses of 400 s.

All the participants to the ITER Project are involved in the procurement of machine components and plant systems. This unique procurement sharing program has an important purpose, allowing all Members to gain direct industrial experience in key fusion technologies. By participating in ITER, the Members are also empowering their scientific, technological and industrial infrastructure with innovative manufacturing processes and cutting-edge technologies in order to achieve the strict requirements set for ITER first of a kind sub-assemblies. Today, in factories on three continents, the components and systems of the ITER plant are taking shape.

Design requirements derived from simulations and modelling have been translated in stringent dimensional and geometrical tolerances which, combined with the dimension of the assemblies and the complex production steps, push the industries to a higher quality standard. In order to comply with these requirements, not only the processes need to be redesigned, but the tools to verify the compliance assume a paramount importance in the production. Metrology, the scientific study of measurement, has a key role in the manufacturing process, since it can help in the monitoring of the evolution of the parts and in the evaluation of the best alignment in between the components towards the final product. Together on-market and tailored tools are integrated in the production, feeding the manufacturing with useful information about the status of the items, helping the decision making in the risk management. The management of the information coming from dimensional

inspections opened the way to the introduction of Digital Twin methodologies and techniques the industry is developing.

The document is divided in five chapters, described below:

- The first chapter concerns some theoretical background of GeoSpelling and Surface Skin Models, and their implementation in Industry 4.0, with a mention to the tools used in the development of the procedure;

- In the second chapter a brief description of the Toroidal Field Coil system and its functioning is presented, to illustrate the method field of applicability;

- In the third chapter a brief description of the Vacuum Vessel and its functioning is presented, to illustrate the method field of applicability;

- The fourth chapter is dedicated to the application of the reconstruction operation to the Toroidal Field coil Winding Pack and the Vacuum Vessel Inner Shell;

- The fifth chapter is dedicated to the application of the association operation to the Toroidal Field coil and the Vacuum Vessel measurements.

Contents

List of figures

List of tables

Acronyms and abbreviations

GD&T	Geometrical Dimensioning and Tolerancing
CAD	Computer Aided Design
CAE	Computer Aided Engineering
CAT	Computer Aided Tolerancing
CPPS	Cyber-physical Production System
M2M	Machine-to-Machine
IoT	Internet of Things
FE	Finite Elements
FEA	Finite Elements Analysis
FEM	Finite Elements Method
RE	Reverse Engineering
PLM	Product Lifecycle Management
TTRS	Technologically and Topologically Related Surfaces
DLM	Direct Linearization Method
SDT	Small Displacement Torsor
CT	Conditional Tolerance
VBR	Virtual Boundary Requirement
TSL	Tolerance Specification Language
GPS	Geometrical Product Specification
GUM	Guide to Uncertainty of Measurements
NURBS	Non-Uniform Rational B-Splines
CCL	Current Center Line
GTAW	Gas Tungsten Arc Welding
NB	Neutral Beam
NDE	Non-Destructive Examination

VV	Vacuum Vessel
RBF	Radial Basis Functions
IS	Inner Shell
TF	Toroidal Field
DP	Double Pancake
VF	Virtual Fitting
WB	Workbench
SA	Spatial Analyzer

1   Digital Twin & Industry 4.0

In the past years, production engineering has been focusing mainly in the Industry 4.0. This term has been introduced in 2015 by Klaus Schwab, the World Economic Forum Founder and Executive Chairman to describe the transition of the industrial environment towards automation and data exchange in manufacturing technologies and processes [1]. Manual data acquisition and variation as part of the layout planning contribute up to 74 % of the overall time consumption during the planning process, thus conflicts with the requirements of near real-time optimization cycles. Traditional methods of process and production planning do not fulfil the demands of near real-time optimization and cannot process the real-time acquired data as a planning basis in a satisfying manner. The Cyber-physical Production System (CPPS) is a core component of Industry 4.0. Its main aims are to provide and enhance transparency in the production system, reduce unscheduled downtime, improve maintenance scheduling and ultimately enhance customer satisfaction. [2]All these objectives can be possible by a real-time production control realization of a Digital Twin, a virtual representation that serves as the real-time digital counterpart of a physical object or process. The concept of digital twins can be broadly applied to many technologies as large-scale machine-to-machine communication (M2M), the internet of things (IoT) computer aided design and engineering (CAD and CAE) and is thus likely to disrupt industries beyond manufacturing. The Digital Twin represents the prerequisite for the development of a CPPS, allowing centralized analysis and control of the production process. Useful provision of data, that were acquired for the development of the Digital Twin, requires a cloud-based solution to ensure a near real-time processing a continuous production system planning is predominant. CAD and CAE model update on manufactured shapes, which are based on Reverse Engineering (RE) techniques, are the core elements of the Digital Twin.

1.1. Introduction and State of the Art

Within the context of Product Lifecycle Management (PLM), information communication and sharing require to manage the geometric variations along the whole product lifecycle. In particular, conceptual and preliminary design phases are two of the more critical ones of the product development process. Decisions and information generated during these phases have large impacts on the succeeding design phases. Therefore, these phases dictate to use methodologies that allow information management, manufacturability or producibility evaluation, preliminary process planning and a cost estimation of the product. There exists a strong need for increased attention to tolerance design to enable high-precision assemblies to be manufactured at lower cost.

To do so, manufacturing activities have to be integrated with conceptual and preliminary designs. This can be possible by the implementation of information management of geometrical variations and tolerancing activities. The purpose of functional tolerancing activity is to define the geometrical specifications of parts ensuring a certain level of quality defined by some product geometrical requirements. It has to take into account the inherent imperfections of manufacturing processes, which cause a degradation of functional characteristics of the product, and therefore, of its quality. [3]

Furthermore, the effects of geometrical specifications impact over other fields of the production, as process planning, manufacturing, quality control and inspection. Therefore, it is important to manage geometrical variations during the whole product life cycle. In addition to preliminary and detailed design other steps of the production needs to be integrated in the geometrical specification: process planning, manufacturing activities, and geometrical inspection.

All these topics have been addressed by the Technical Committee for the development of the GPS standards ISO 17450-1 [4]. Dimensional and Geometrical Product Specifications and Verification, which focuses on the Geometrical Part Specification model.

In a typical Tolerancing Process, applied from the early conceptual stage of the design process to the final detailed design, geometrical product requirements have to be expressed to ensure the continuous transition from functions to functional part tolerances. In this context, geometric dimensioning and tolerancing (GD&T) during product development is the first step in geometric variations management. It aims at ensuring an adequate product quality level considering tolerance-related manufacturing and inspection costs by setting limits for manufacturing-caused geometric imperfections. [5]

In this regard, the basic tolerancing tasks in design are tolerance specification, tolerance allocation, and tolerance analysis. Nowadays, computer aided tools support the product developer in these activities for geometric product specification and tolerancing. In the context of Computer-Aided Tolerancing (CAT), many CAT tools can help designers for functional tolerance specification such as vectorial tolerancing [6], the model of Technologically and Topologically Related Surfaces (TTRS) [7], the Direct Linearization Method (DLM) [8], Tolerance-Maps [9], or the Deviation Domain [10] based on the Small Displacement Torsor (SDT) [11].

However, they are limited to control the geometric variations when covering the whole product lifecycle.

Hillyard and Braid developed the concept of variational geometry [12] that is a dimension-driven, constraint-based technique. Another early example of previous work of tolerance-modelling technique is the solids offset approach proposed by Requicha [13], in which the tolerance zones of workpieces are obtained by ''offsetting'' the nominal boundaries. Bourdet [14] developed the concept of the Small Displacement Torsor (SDT) to solve the general problem of the fit of a geometric surface model to a set of points using rigid body movements. Based on the solids offset approach, Jayaraman and Srinivasan proposed Virtual Boundary Requirement (VBRs) and Conditional Tolerance (CTs) approach ([15], [16]). Etesami [17] formalizes the solids offset model and proposed using Tolerance Specification Language (TSL) to describe tolerance constraints. Shah et al. [18] proposed a dimension and geometric model, which is based on the relative degrees of freedom of geometric entities: feature axes, edges, faces, and features-of-size. Roy et al. [19] presented a mathematical scheme for interpreting dimensional and geometric tolerances for polyhedral parts in a solid modeler [20]. In the past,

these models have mainly been used for assembly-oriented tolerance analysis, i. e., analysing the effects of part tolerances on assembly gaps and clearances, rather than for functional tolerancing. However, there is a growing interest in considering working conditions and operating windows in CAT. Though, many of these computer models for tolerance simulation and analysis disregard environmental impacts and different sources of deviations. Furthermore, most of these models make severe simplifications about observable geometric deviations since they are reduced to rotational and translational feature defects.

Therefore, geometric tolerances are modelled instead of geometric deviations in a strict sense. This leads to results with large ranges of uncertainty and a discrepancy between the virtual models and the observed reality. Furthermore, the tolerancing tasks in design as well as all other activities of geometric variations management should be incorporated in a complete and coherent tolerancing process.

1.2. GeoSpelling and Skin Model

As a response to these needs, Ballu and Mathieu proposed GeoSpelling ([20], [21]) as an univocal language, which is common to design, manufacturing, and inspection and allows the communication of geometric information and requirements along the product life cycle.

This language has been adopted by the ISO in the standards for the Dimensional and Geometrical Product Specification and Verification (GPS) recently.

A basic concept within GeoSpelling and the ISO standards is the Skin Model Concept, which is an infinite model of the physical interface between the workpiece and its environment.

The description of GeoSpelling allows a unified description of geometrical specification. The mathematical model has to express the "real-world" of the product with the minimum of uncertainty; the aim is to reduce risk of misinterpretations and ambiguities.
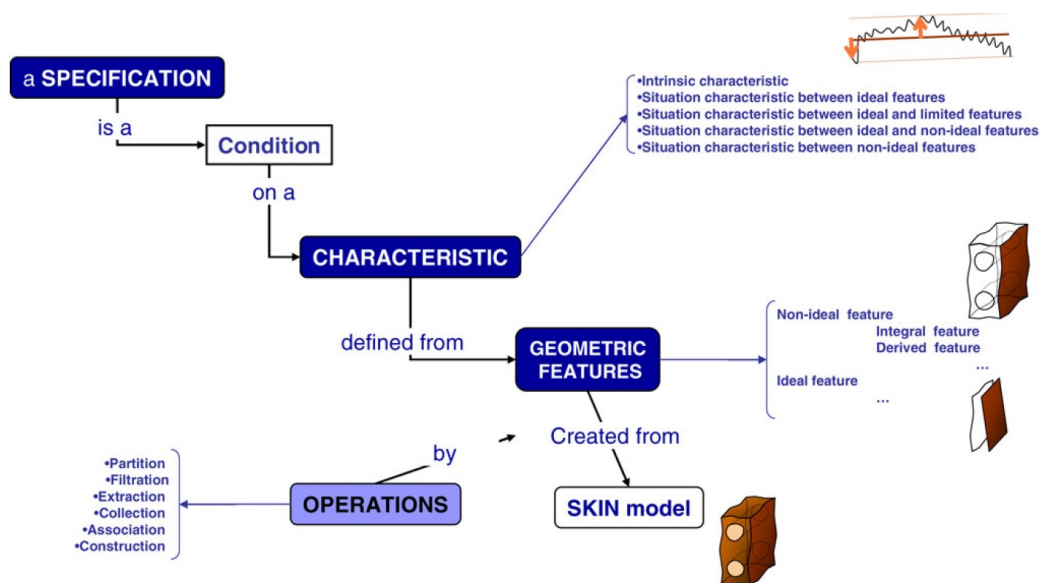
Figure 1: Elements of the Skin Model [3]

The idea behind this framework is to create part representatives with geometric deviations depicted as Skin Model Shapes. By employing computer aided engineering methods for assembly and use, the effects of geometric deviations on assemblability as well as the product's functional behaviour can be analysed.

Several elements have to be introduced to describe the Skin Model Concept (Figure 1). From the nominal model to the non-ideal surface model, which introduce the deviations in the ideal design world, passing through the prediction and observation stages of the manufacturing process, in which the estimation of the error and the actual measured deviation define the corresponding models to the feature and operations that defines all the mentioned models will be presented in the following section.

1.3. Nominal and Non-Ideal Model

In the preliminary and advanced design stages, the designer specifies a "workpiece" with a perfect form, i.e. with the shape and dimensions necessary to meet the functional requirements. This workpiece is called the "nominal model" (see **Figure 2**).

This first step establishes a representation of the workpiece with only nominal values that is impossible to produce or inspect (each manufacturing or measuring process has its own variability or uncertainty).

The real surface of the workpiece, which is the physical interface of the workpiece with its environment, has an imperfect geometry; it is impossible to completely capture the dimensional variation of the real surface of the workpiece in order to completely understand the extent of all variation.

From the nominal geometry, the designer imagines a model of this real surface, which represents the variations that could be expected on the real surface of the workpiece. This model representing the imperfect geometry of the workpiece is called the "non-ideal surface model" (see **Figure 2**).
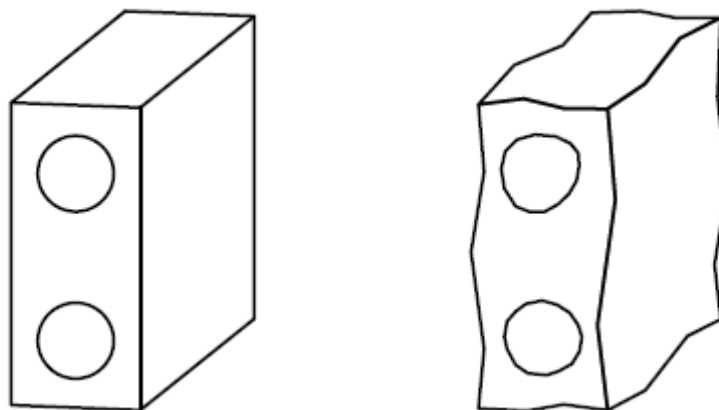
Figure 2: Nominal model (left) and Non-ideal surface model (right) [4].

The non-ideal surface model is used to simulate variations of the surface at a conceptual level. On this model, the designer will be able to optimize the maximum permissible limit values for which the function is downgraded but still ensured. These maximum permissible limit values define the tolerances of each characteristic of the workpiece.

At this stage, the Skin Model is an infinite model and does not allow to link the reality of the workpiece to it, since the theoretic workpiece surface comprises an infinite number of points. The infinite description is required in the simulation world to be able to consider all kinds of geometric deviations, from a macro to a nano scale, and to capture these different variations. It is not possible to clearly define geometric specifications and to enable an unambiguous product development process at a conceptual level without the infinite description. However, a finite description has to be available in order to compute and to process the Skin Model. This leads to the idea of Skin Model Shapes, which are particular finite Skin Model representatives comprising a finite number of geometry parameters or points. Thus, a Skin Model Shape is a specific finite Skin Model outcome and comprises deviations from manufacturing and assembly. Due to the different scale of geometric deviations, the number of possible Skin Model Shapes is very high, they are virtually limited only by the level of detail that is to be achieved. If these Skin Model Shapes are sufficiently precise, then all relevant kinds of geometric variations can be captured.

At a conceptual level, Skin Model Shapes are not related to a specific geometry representation scheme, such as discrete or parametric. Therefore, the concept allows a holistic and persistent geometric deviations management process, in contrast to other models, such as the Geometric Deviation Model, which only considers rotational and translational feature defects from manufacturing and assembly and does not take into account other kinds of geometric deviations and deformations arising during usage.

1.4.   Prediction and Observation

It seems appropriate to split the process of Skin Model Shape simulation in two phases regarding the current status in product development and to develop a Skin Model Shape simulation approach for each of these two stages:

- In early engineering design stages, geometric deviations of the relevant part are not yet observed. Therefore, assumptions on systematic and random deviations should be incorporated for predicting Skin Model Shapes. This stage may be referred to as the "Prediction Stage".
- During later design stages, manufacturing process simulations and even prototypes of the part may be available. Thus, these observations should be taken into consideration and possible outcomes of the production process based on few samples should be simulated. This stage may be referred to as the "Observation Stage" accordingly.

In general, the generation of Skin Model Shapes in early design stages builds up on the nominal model (e. g. provided by CAD systems). The geometric data are then enhanced with information about the systematic deviations, which are likely to occur through a certain production process. Following that, random deviations are added to the model. Two main axioms cover these geometric deviations, namely the axiom of manufacturing imprecision and the axiom of measurement uncertainty, which are described in section 1.8.

The operationalization of the Skin Model concept into a discrete geometry framework is highly based on the generation of realistic representatives of the workpieces showing observable geometric deviations. These generated Skin Model Shapes can then be used in various engineering simulations, such as assembly analysis or tolerance simulations for predicting the later product behaviour. For this purpose, the Skin Model Shape simulation approaches should incorporate all available information about the actual shape and dimensions as well as the expectable geometric deviations of the workpiece.

1.5. Features

Features are elements that can be used to describe all the models introduced in the previous section. According to the definition of a geometrical feature, its nature is a point, line, surface or volume. Two kinds of geometrical features can be distinguished:

- ideal features
- non-ideal features

Ideal features are defined by type and by intrinsic characteristics. An ideal feature is generally referred to by its type, for example, straight line, plane, cylinder, cone, sphere or torus. Characteristics are the variables that define a certain type of feature. An example of an intrinsic characteristic is the diameter of a cylinder. Ideal features used to define the nominal model are called "nominal features". These are independent of the non-ideal surface model. Ideal features whom characteristics are dependent on the non-ideal surface model are called "associated features".For instance, the nominal model shown in Figure 3 is built with several ideal features of two types (plane and cylinder). The locations and orientations between the features are given by situation characteristics, and the diameters of the cylinders are given by intrinsic characteristics.

a) Nominal model   b) Ideal features of types plane (PL) and cylinder (CY) constituting the nominal model
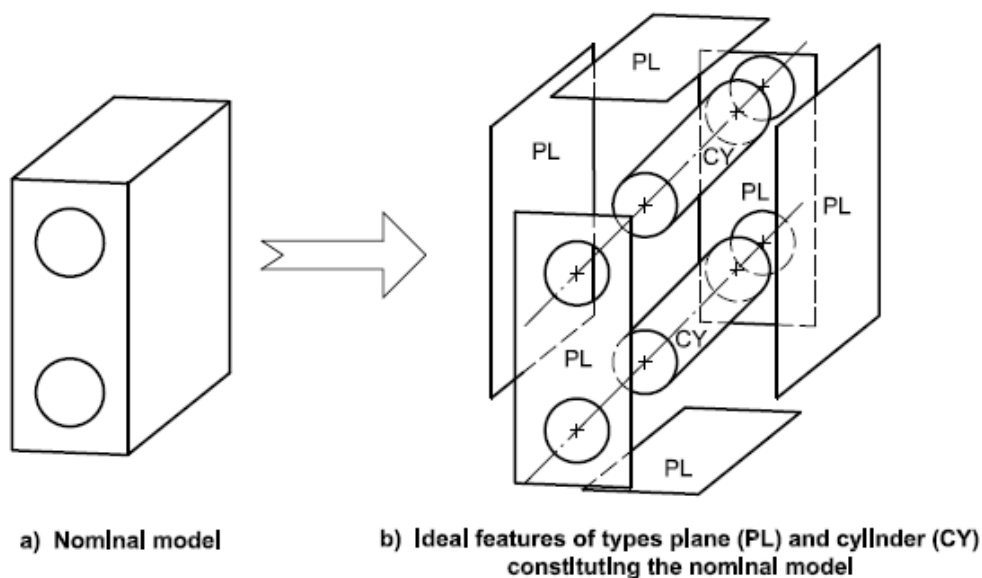
Figure 3: Non-ideal surface model *[4]*.

Non-ideal features are fully dependent on the non-ideal surface model. They can be:

- the non-ideal surface model itself,
- part of the non-ideal surface model, called partition features,
- the derived partition features: features not included in the non-ideal surface model but created through an operation from partition feature, or the intersection between the non-ideal surface model and an ideal feature (Figure 4).
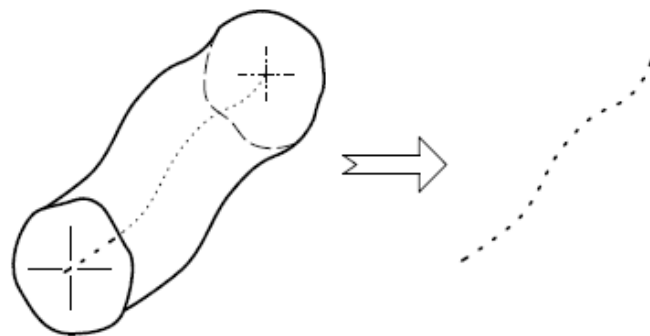
Figure 4: Derived partition feature [4].

Non-ideal features are bound and are composed of an infinite or finite set of points. The relationship between geometrical feature definitions (illustrated in Figure 5) shows the possible complexity when the real workpiece or the non-ideal surface model – not the nominal model – is considered. The objective of GPS specifications is to define with the least ambiguity possible the intended characteristic to be evaluated either from one geometrical feature or between geometrical features, by specifying the characteristic and the geometrical feature from the real workpiece or its non-ideal surface model.
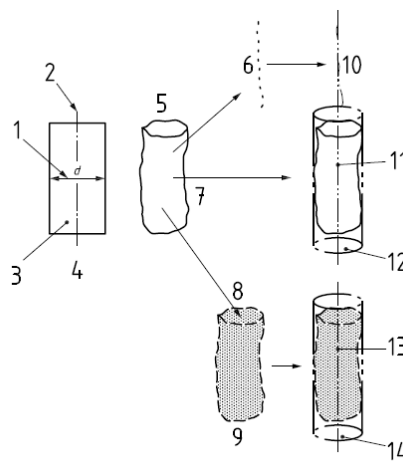
Figure 5: Relationships between geometrical features [4].

Key

1. size of the feature of size
2. nominal median feature
3. nominal integral surface
4. nominal model of the surface
5. non-ideal model of the surface representing
6. non-ideal median feature
7. non-ideal integral surface
8. extraction

9. non-ideal integral extracted surface
10. indirectly associated median feature
11. directly associated median feature
12. surface the real surface of the workpiece
13. ideal directly associated integral
14. directly associated median feature
15. ideal directly associated integral surface

Table 1: Type of geometrical features and associated qualifiers [4].

Taken from	Real surface of the workpiece	Surface model		
		Nominal model	Non-ideal surface model	
Illustration				
Integral feature	Real feature	Nominal integral feature	Example: extracted integral feature	Associated integral feature
Derived feature		Nominal derived feature	Example: extracted derived feature	Associated derived feature
Qualifier	Real	nominal	Examples: extracted; filtered; reconstructed	Associated
Type of geometrical feature	Non-ideal	Ideal	Non-ideal	Ideal

1.6. Operations

Various operations such as partition, extraction, filtration, association, collection and construction are required to obtain certain ideal or non-ideal geometric features [4].

Partition is the operation that identify a portion of a geometrical feature. It is used to obtain, from the non-ideal surface model or real surface, the non-ideal features corresponding to the nominal features (see Figure 6). It is also used to obtain limited parts of ideal features (e.g. a segment of a straight line) or non-ideal features (e.g. a section of a non-ideal surface). For each non-ideal feature, there is a corresponding ideal feature (e.g. ideal plane and ideal cylinder) of the nominal model (compare Figure 3 and Figure 6). The non-ideal features are obtained from the non-ideal surface model, in accordance with specified criteria.

a) Skin model   b) Non-ideal features obtained by partition of skin model
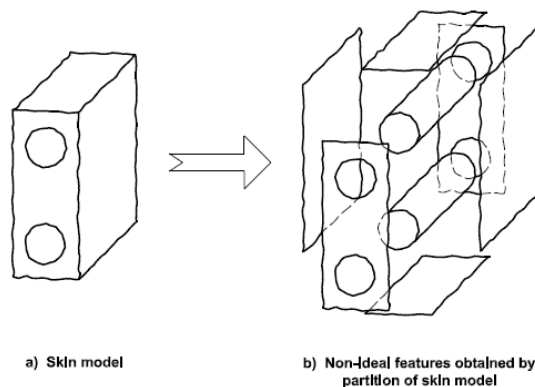
Figure 6: Partition of a non-ideal surface model [4].

Extraction is the operation used to distinguish between roughness, waviness, structure and shape etc. (see Figure 7). This operation permits the obtaining, from a non-ideal feature, of the feature that represents the considered characteristics. This operation is done in accordance with specified criteria.

a) Unfiltered profile   b) Waviness profile   c) Roughness profile
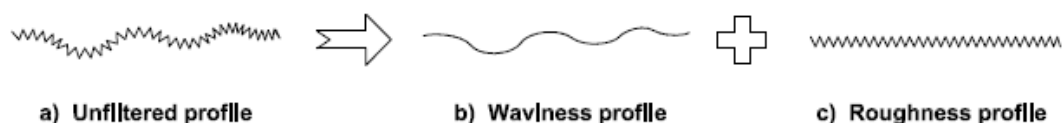
Figure 7: Example of extraction of a profile [4].

Association is the operation used to fit ideal features to non-ideal features in accordance with specified criteria (see Figure 8).The criteria of association give an objective for a characteristic and can set constraints. The constraints fix the value of the characteristics or set limits to the characteristic.

a) Non-ideal feature

b) Ideal cylinder

c) Association of ideal cylinder with the non-ideal feature having criterion "maximize the diameter of the inscribed cylinder"
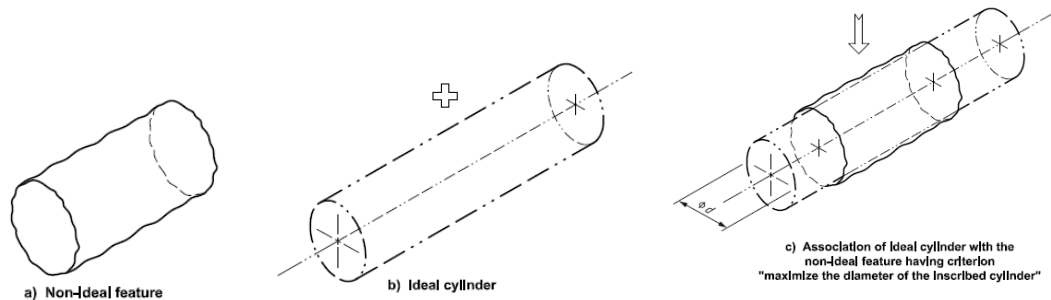
Figure 8: Example of association [4].

Constraints can apply to intrinsic characteristics, situation characteristics between ideal features, or situation characteristics between ideal and non-ideal features. An ideal feature is associated to the non-ideal feature; for example, in the case of a cylinder, the association criteria could be:

- minimize the sum of the squares of the distance between each point of the non-ideal feature to the ideal cylinder, or
- maximize the diameter of the inscribed cylinder (see Figure 8), or
- minimize the diameter of circumscribed cylinder, or
- other criteria.

Collection is the operation used to identify and consider some features together which together play a functional role (see **Key**

CY1: ideal cylinder 1

CY2: ideal cylinder 2

Figure 9). It is possible to build the collection of ideal features or the collection of non-ideal features.

In **Key**

CY1: ideal cylinder 1

CY2: ideal cylinder 2

Figure 9, two parallel cylinders (whose axes lie in a plane and are parallel) are considered together (e.g. for building a common datum). The feature collection of the two cylinders is to be defined. This collection of two cylinders is only invariant by translation along a straight line. It belongs to the prismatic invariance class.

Key
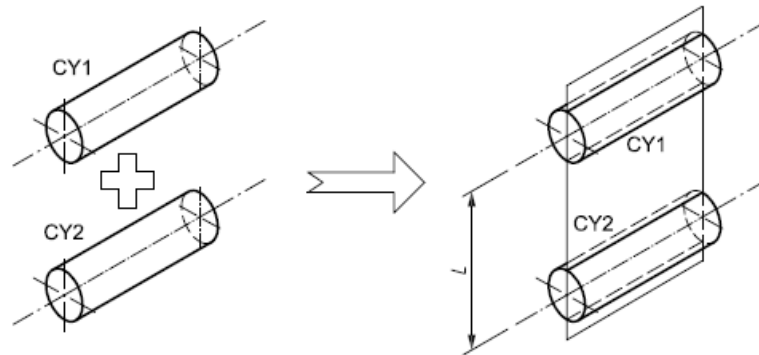
CY1: ideal cylinder 1

CY2: ideal cylinder 2

Figure 9: Example of collection of two ideal cylinders [4].

Construction is the operation used to build ideal features from other features (see Figure 10). This operation shall respect constraints.
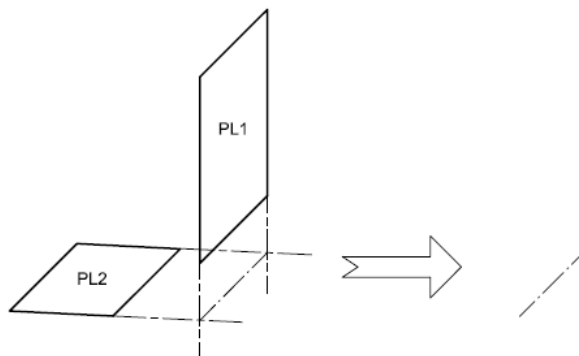
Key

PL1 ideal plane 1

PL2 ideal plane 2

Figure 10: Example of construction of a straight line by the intersection of two planes [4].

Reconstruction is the operation used to create a continuous feature (close or not) from a noncontinuous feature (e.g. extracted feature) (see Figure 11). There are several type of reconstructions. Without this type of operation, it is not possible to define an intersection between an extracted feature and an ideal feature (this intersection could result in the empty set of points).

Key

1. extracted feature (non-continuous feature)
2. reconstructed feature (continuous feature)

Figure 11: Example of reconstruction [4].

These operations are described and defined in GeoSpelling and can be applied to the nominal model as well as to the Skin Model.

1.7. Tools for Skin Model Shapes

Modern computer aided simulation tools in engineering applications are highly based on the representation of physical objects and solid modelling [22]. Common representation schemes for three-dimensional models are wire frames, surface models, volume models, and cell models [23]. As described in the previous section, passing from the infinite model to the finite model, there are virtually infinite Skin Models representing the same real component. Representation schemes of Discrete Geometry such as point clouds and surface meshes are commonly used as surface models. They are straightforward and seem to be adequate for the representation of deviated workpiece representatives. Therefore, a point-based representation is often used for modelling geometric deviations. A point cloud can be defined as a set of vertices in a three-dimensional coordinate system, which are usually defined by X, Y and Z coordinates. Typically, a point cloud is intended to represent the surface of a solid object. The representation of the object's surface by a point cloud offers advantages but also implies some limitations. The point cloud concept is quite simple and involves little conversion problems when using different software tools. Furthermore, point cloud formats are commonly created by 3D scanners in manufacturing and metrology/quality inspection applications. However, point clouds themselves are already an approximation of the real surface of the object. Within the instrument capabilities, the level of approximation, and consequently the detail of geometric deviations that will be represented in the Skin Model, can be adjusted by the point density.

A surface mesh of the object can be created from a point cloud via triangulation. This offers possibilities to approximate the surface of the object for visualization and further processing. These geometric imperfections of surfaces can be roughly classified into lay, waviness, and roughness. These classes of geometric deviations differ in terms of the relationship between distance and depth of the imperfections. However, this classification is not disjunct.

Moreover, other surface models can be processed from the point cloud through surface reconstruction methods.

The described geometric deviations can furthermore be distinguished between systematic and random deviations. This classification is based on the experience, that in many manufacturing processes, similar geometric deviations can be observed on every part whereas some geometric deviations can be observed only on a few workpieces. The systematic deviations are deterministic, predictable, and reproducible and may be depending on the manufacturing process, such as products of clamping errors or the machine dynamical behaviour. In contrast to that, random deviations arise from fluctuations of the production process such as tool wear, varying material properties or fluctuations in environmental parameters (temperature, humidity, etc, ...). In order to extract valuable information from these Skin Model Shapes in engineering design, visualization techniques have to be employed, which illustrate geometric deviations and make them visible.

Coming from a point-based geometry representation, a straightforward idea for the visualization of geometric deviations of Skin Model Shapes is to determine the distances between the points of the nominal model and the Skin Model Shape. These distances have then to be converted to a RGB colour scale. Furthermore, the point distances may be weighted according to their spatial direction, for example in the direction of the vertex normal. For this purpose, the point distances between the nominal model and the Skin Model Shape are only computed in the local vertex normal direction. These local vertex normals can also be used to determine a deviation volume, which is composed by the vertex normals of the nominal model and those of the Skin Model Shape [5].

1.8. Uncertainty and Error

Another element which determines the quality of the representation of the reality with the skin model is the measurement uncertainty. It is a parameter, associated with the result of a measurement, that characterizes the dispersion of the values that could reasonably be attributed to the measurand. Every measurement process has its own uncertainty associated to it. The Guide to Uncertainty of Measurements (GUM) [24] gives indications on how to evaluate this value by combining the effect of the several uncertainty sources, and to plan the measurement campaign in order to minimize the impact of this error in the virtual representation of reality.

The uncertainty in measurement is usually a result of the combination of several different effects. Each of these effects can confer errors on a measured value or contribute to the uncertainty of the measured value. The origins of errors and uncertainty can include:

- The measuring instrument: may suffer from errors
- The item being measured: may change over time
- The measurement procedure: may be difficult to perform
- Imported uncertainties: from calibrations, or other information that helps you arrive at your measured value, for example, through calculations
- Operator skill: some measurement processes require dexterity experience and judgment
- Sampling issues: can mean what you are measuring is not representative of the whole; it is important to specify the measurand unambiguously
- The environment: some measurements are affected by varying ambient conditions.

The two components directly related to the measurement uncertainty and errors are accuracy and precision:

- Accuracy: a qualitative term describing the closeness of a measured value to the true value

- Precision: refer to the dispersion of a number of measured values when the measurement is repeated
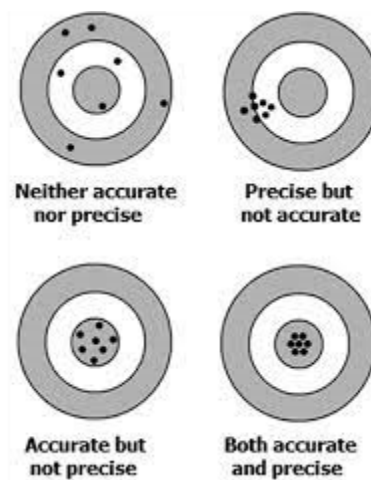
Figure 12: Precision and accuracy [Retrieved on 21 Jul 2022 on www.npl.co.uk]

Another classification of measurement uncertainty components, includes systematic measurement error, which is the component of measurement error that in replicated measurements remains constant or varies in a predictable manner, in general it is associated with corrections and the assigned quantity values of measurement standards, as well as the random measurement error, an error component of measurement that in replicated measurements varies in an unpredictable manner, to which a definitional uncertainty is associated.

Sometimes estimated systematic effects are not corrected for but, instead, associated measurement uncertainty components are incorporated.

1.9. Bezier Curves and NURBS

Non-Uniform Rational B-Splines, commonly referred to as NURBS, is a mathematical model using basis splines (B-splines) that is commonly used in computer graphics for representing curves and surfaces [25]. They have become the *de facto* industry standard for the representation, design, and data exchange of geometric information processed in CAD, CAM and CAE. Indeed they are, together with cloud points and surface meshes, the representation of the Skin Model Shapes.

Many national and international standards, e.g., IGES, STEP, and PHIGS, recognize NURBS as powerful tools for geometric design. The enormous success behind NURBS is largely due to the fact that:

- NURBS provide a unified mathematical basis for representing both analytic shapes, such as conic sections and quadric surfaces, as well as free-form entities, such as car bodies and ship hulls;
- They can be efficiently handled by computer programs yet allow for easy human interaction.
- NURBS algorithms are fast and numerically stable;
- NURBS curves and surfaces are invariant under common geometric transformations, such as translation, rotation, parallel and perspective projections;

The excellent mathematical and algorithmic properties, combined with successful industrial applications, have contributed to the enormous popularity of NURBS.

NURBS surfaces are functions of two parameters mapping to a surface in three-dimensional space. The shape of the surface is determined by control points. In a compact form, NURBS surfaces can represent simple geometrical shapes.

In general, editing NURBS curves and surfaces is intuitive and predictable. Control points are always either connected directly to the curve or surface. Depending on the

type of user interface, the editing of NURBS curves and surfaces can be via their control points (similar to Bézier curves) or via higher level tools such as spline modelling and hierarchical editing.

A NURBS curve is defined by its order, a set of weighted control points, and a knot vector. NURBS curves and surfaces are generalizations of both B-splines and Bézier curves and surfaces, the primary difference being the weighting of the control points, which makes NURBS curves rational. By using a two-dimensional grid of control points, NURBS surfaces including planar patches and sections of spheres can be created. These are parametrized with two variables (typically called s and t or u and v). This can be extended to arbitrary dimensions to create NURBS mapping. The order of a NURBS curve defines the number of nearby control points that influence any given point on the curve. The curve is represented mathematically by a polynomial of degree one less than the order of the curve. Hence, second-order curves (which are represented by linear polynomials) are called linear curves, third-order curves are called quadratic curves, and fourth-order curves are called cubic curves. The number of control points must be greater than or equal to the order of the curve.

1.10. RBF mesh morphing

The RBF technique has been proven to be a reliable and flexible method to interpolate discrete values (loads, displacements, etc.) over a certain field [26] [27] [28] [29]. Before being used in the CAD update, the RBFs technique has been deployed in several other fields, including meshless Fracture Mechanics (FM) [30] and FEM results improvement [31]. In this section, a brief description of RBFs is given to introduce the morphing technique adopted in the following paragraphs. Dedicated textbooks provide a wider description of mathematical background on RBFs, along with their applications [32] [33] [34]. In the early 60s, problems of multidimensional interpolation have been tackled with the introduction of RBFs [35]. From a series of N scattered scalar values attributed to their respective points x_{ki} in the space $\mathbb{R}$ (called source points), an approximating smooth function can be constructed in the same space with the usage of an interpolator s. At a location x its value is:

$$s(x) = \sum_{i=1}^{N} \gamma_i \varphi\left(\left\| x - x_{k_i} \right\|\right) \tag{1}$$

Having the function available, a corresponding value can be retrieved in a different point from the source in the space of the function. The variable φ is attributed to the radial function, a scalar function based on the Euclidean distance between the source and target points. γ_i are weights of the radial interactions whose order is equal to the number of source points introduced. For the computation of the weights, a linear system of equations needs to be solved. Typical radial functions are collected in the table below (Table 2), for $r = \| x - x_{ki} \|$:

Table 2: Radial Basis Functions

RBF	Column A (t)
Spline type (Rn)	r^n, n odd
Thin plate spline	$r^n log(r)$, n even
Multiquadric (MQ)	$\sqrt{1 + r^2}$
Inverse multiquadric (IMQ)	$\dfrac{1}{\sqrt{1 + r^2}}$
Inverse quadric (IQ)	$\dfrac{1}{1 + r^2}$
Gaussian (GS)	e^{-r^2}

$$\begin{cases} s_x(x) = \sum_{i=1}^{N} \gamma_i^x \varphi(\|x - x_{k_i}\|) + \beta_1^x + \beta_2^x x + \beta_3^x y + \beta_4^x z \\ s_y(x) = \sum_{i=1}^{N} \gamma_i^y \varphi(\|x - x_{k_i}\|) + \beta_1^y + \beta_2^y x + \beta_3^y y + \beta_4^y z \\ s_z(x) = \sum_{i=1}^{N} \gamma_i^z \varphi(\|x - x_{k_i}\|) + \beta_1^z + \beta_2^z x + \beta_3^z y + \beta_4^z z \end{cases} \quad (2)$$

Metrology techniques usually provide the information needed in the form of cloud points from which triangular tessellated surfaces generate. The input STereo Lithography (STL) is the target of the morphing action.

2 The TF Coils

In this section, a description of the Toroidal Field (TF) coils will be given. The technical challenges as well as the production will be introduced, in order to give a context in which the exercises of association and reconstruction of skin model shapes have been carried out. In the European roadmap for the realization of a commercial Fusion Power Plant [36], high performances have been set up for the ITER Tokamak fusion reactor. The tokamak has to produce a peak magnetic field of around 12 T in order to confine the high temperature plasma (150M C°).
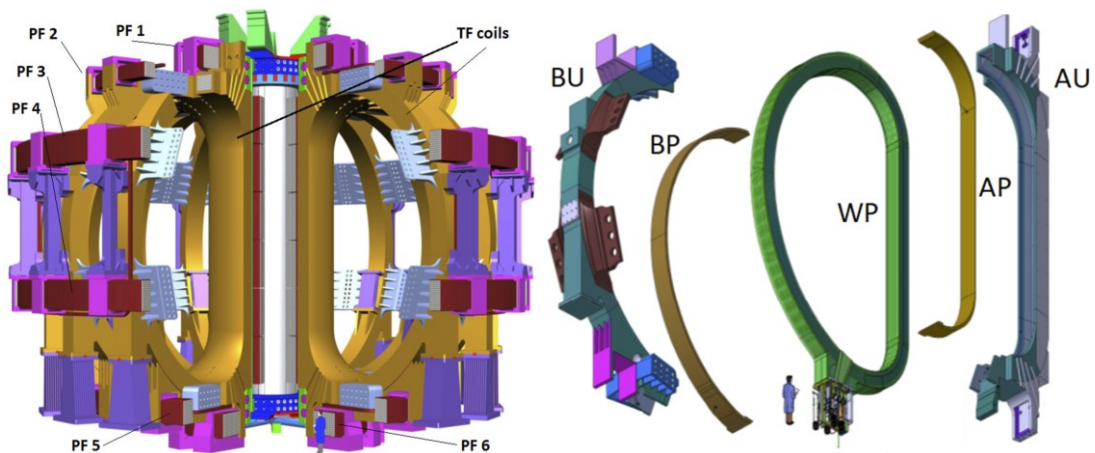
Figure 13: TF coil system assembly [37].

To achieve such goal ITER includes 3 principal superconducting magnet systems. They are as in Figure 13, the Central Solenoid, Poloidal Field (PF) and Toroidal Field (TF) coil systems.

The TFC system consists of 18 D-shape winding packs (WP), enclosed in SS316LN cases (TFCC), which provide structural integrity and isolation to the superconductors, while assuring the connection to other components of the ITER machine. Each TFC is approximately 16.5 m × 9 m in size and 300 t in weight. In order to confine the plasma they are operated at a constant 68 kA and 11.8 T peak field.

2.1. TF components and manufacturing

The principal subassemblies of each coil are a thick stainless steel Coil Case (CC), composed of 4 subassemblies into which a Winding Pack (WP) is inserted (Figure 13). The WP is comprised of a stack of 7 Double Pancakes (DP). In turn, the main components of each DP are a stainless steel Radial Plate (RP) and unit length of Nb3Sn Cable in Conduit Conductor (CICC) (Figure 14).

Figure 14: Winding Pack [Retrieved on 21 Jul 2022 on www. fusionforenergy.europa.eu]

The main parameter of the quality of each TFC system is the Current Center Line (CCL). The CCL is the geometrical centre of gravity of the conductors inside a WP: it is a simplified representation of the current distribution of the currents circulating in the 144 turns of the WP. The as-built CCL of a WP is calculated on the basis of the measured geometrical position of the DPs [38] [39]. The accuracy of its position in a TF is essential to produce a homogenous magnetic field. The main requirement for the CCL position inside a TF coil is an accuracy of $+/-1.25$ mm on the straight leg of the D-shaped coil. Such accuracy depends on several factors: the conductor trajectory

inside a DP, the accuracy of the DPs position inside the WP and the accuracy of the positioning of the WP inside its CC. Considering the large dimensions of a TF coil and the complexity of the manufacturing process, this requirement is very demanding.

In the Tokamak, the TF coils are mechanically connected to a number of other large components, such as the adjacent TF coils, PF coils, thermal shield and others. The ITER Organization (IO) has defined tolerances for each of these components which are built by different suppliers around the world. Due to their large dimensions, it is not possible to modify such components during assembly. It is therefore essential to respect the required tolerances during the TF coils production. A proper manufacturing plan, which will be described in the following section, has been set up in order to meet this requirement.
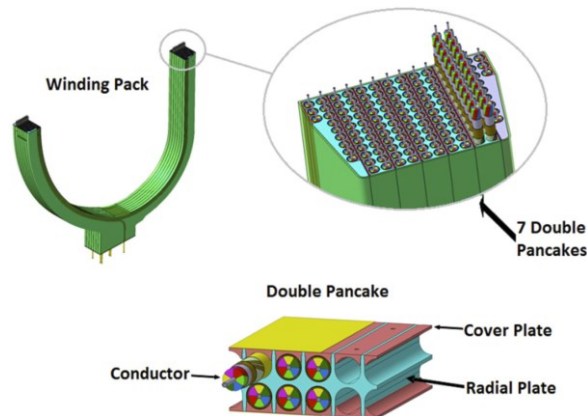
Figure 15: Winding Pack sub-assembies *[37]*

The WP manufacturing starts from the conductor cable assembly. The conductor is formed by 1400 cables of superconducting Nb_3Sn and Cu strands fitted inside a Stainless Steel (SS) cable of about 45 mm in diameter. After being heat-treated at 650 ºC in an inert atmosphere, the 750 m of the conductor are bent into a double spiral trajectory and then fitted inside the radial plate, which is represented by an SS structure with grooves on both sides. The sub-assembly is afterward locked by SS cover plates, which are laser welded by three robots working simultaneously to form a Double Pancake (DP). After being wrapped in the insulating tape and impregnated with resin, the component is cured at high temperature. Seven double pancakes are after that stacked, electrically jointed, wrapped and finally electrically insulated with

glass Kapton tape to form the WP. The component undergoes another impregnation cycle before being finalized. Before the delivery, a series of final tests are carried out, including dimensional checks. (Figure 15)

For the component, a full 3D scan is performed at the end of the production, in order to certify the external surface quality, the final dimensions of the superconductor and the interfaces in the terminal area.

Each WP has to be inserted inside its CC. The process starts with the Acceptance and testing of the four sub-assemblies. Once arrived, the CC are visually checked and then positioned in the DI room (**Figure 16**) and thermalized at 20 °C $\pm$ 2 before to perform the dimensional inspection. Particular attention is paid to measure the inner surfaces of the CC, facing the WP, and the welding bevels, which will be used in the assembly simulation. After this, a leak test is performed. For this test the searching vacuum is the inner volume of the cooling pipes and the CC are wrapped with plastic bags inflated with helium.

Figure 16: Coil Cases acceptance [37].

Once the tests are successfully passed the CCs are positioned in the Insertion Tooling or "Assembly Rig" (AR), where the insertion of the WP into the CC is achieved. 11

bottom pads of the WP-CC contact interface and 6 lateral bumpers are custom designed and installed on AU side using the dimensional inspection data of the surfaces of the WP and the corresponding surfaces of the CC. These two types of spacer lock the position of the WP in the TFC. The insertion of the WP into the CC is done in a horizontal configuration. The WP is kept in position by 11 pushers (**Figure 17**) and each of the 11 pads is placed on a sliding support that is moved backwards while the CCs (AU and BU) are approached towards the WP. The supports, on which the WP is loaded, slide on the CC surface and the WP weight passes from the WP supports to the CC supports. Once the WP insertion is completed the two closing plates AP and BP are positioned.
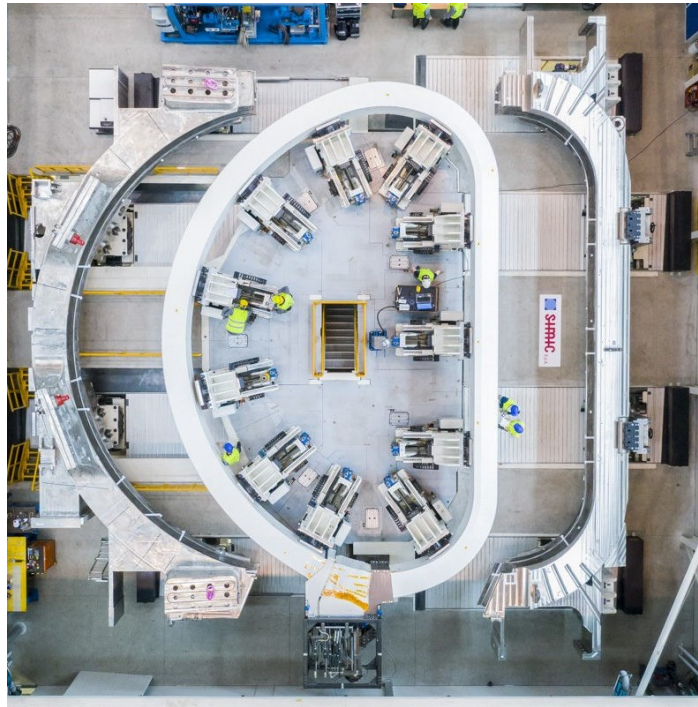
Figure 17: Coil Cases and WP assembly [37].

Once the closure plates have been positioned, the closure of the cases by welding can start. All the welding process are GTAW; for the AU-BU weld (about 90 mm thick) a manual process was chosen for accessibility reasons and for the poloidal weld (AU-AP and BU-BP, thickness varying from 40 mm to 120 mm) an automatic Narrow-Gap pulsed GTAW is used (**Figure 18**). The poloidal welding is performed using two welding robots at the same time.

Figure 18: Coil Cases welding [37].

Once the closure has been completed, the coil is tilted with an angle of 5 degrees in order to inject approximately 1.500 l of resin which will fill the remaining gaps between the WP and the cases. After being hardened by heating, the assembly is achieved (**Figure 19**).
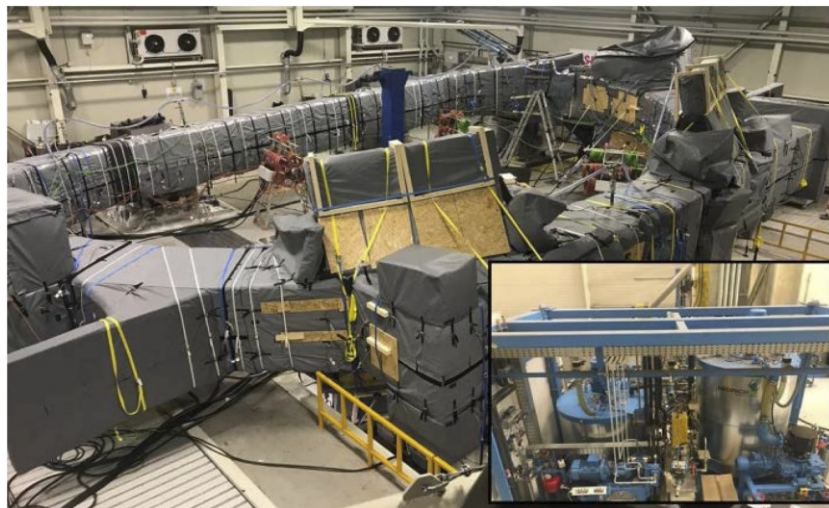
Figure 19: Impregnation [37].

The TFC interfaces are finally machined to fix the CCL in the correct position with respect to the tokamak reference, and the final tests are performed before delivery.

3   The Vacuum Vessel

In this section, a description of the Vacuum Vessel (VV) will be given. The technical challenges as well as the production will be introduced, in order to give a context in which the exercises of association and reconstruction of skin model shapes have been carried out.

The ITER experiments will take place inside the VV, a hermetically sealed steel container that houses the fusion reactions and acts as a first safety containment barrier. In its doughnut-shaped chamber, or torus, the plasma particles spiral around continuously without touching the walls.

The vacuum vessel is one of the key components of the reactor. It performs multiples functions, namely:

- provides a boundary consistent with the generation and maintenance of a high-quality vacuum, necessary for limiting impurity influx into the plasma;
- supports the in-vessel components and their resultant mechanical loads; ·
- participates in shielding against neutrons, and in removing the corresponding power during a pulse, and moreover in removing the decay heat of all in-vessel components in case of there being no other coolant available;
- provides a continuous conductive shell for plasma stabilisation with a toroidal one turn resistance of ~8mW; ·
- provides all access to the plasma through ports, for diagnostics, heating systems, pumping, water piping, etc.;
- provides the first confinement barrier for tritium and activated dust with a very high reliability.
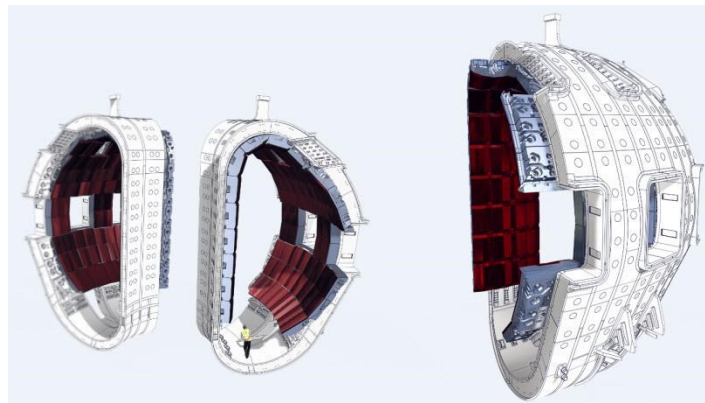
Figure 20: ITER Vacuum Vessel sector. [Retrieved on 21 Jul 2022 on www.iter.org]

All these functions are central to the operation of ITER and thus require a very robust mechanical design in all possible normal and off-normal conditions. The vessel is made by two shells linked via structural ribs and fitted with nuclear radiation shielding material.

To ensure reliable water cooling, two independent forced convective loops are used. These can also remove by natural convection the decay heat from all in-vessel components (if they are not cooled directly). The vessel water temperature is maintained at around 100°C limiting to ~50°C its difference with the in-vessel component cooling temperature.

The VV is located inside the cryostat and supported by the vessel gravity supports

The blanket and divertor are mounted on the vessel interior and all loads are transferred to the vessel. The blanket modules are supported directly by the VV and the blanket cooling channels are routed over its plasma-side surface. The basic configuration and poloidal cross-section of the VV are shown in Figure 21. Detailed parameters are summarized in Table 3.
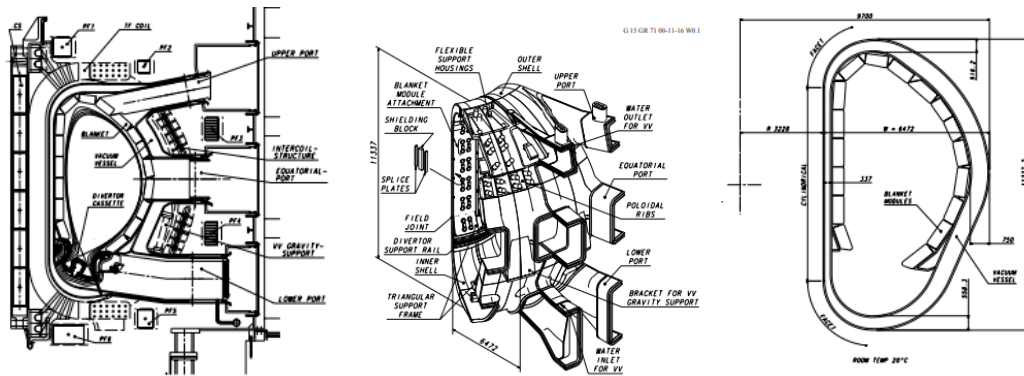
Figure 21: Tokamak poloidal cross section (left), Vacuum Vessel arrangement (center) and cross section (right) *[40]*.

The VV has upper, equatorial, and lower port structures used for equipment installation, utility feedthroughs, cryo-vacuum pumping, and access inside the vessel for maintenance. Most of the port components are also of double wall construction with stiffening ribs between the walls.

Table 3: Main VV parameters *[41]*.

Vacuum vessel parameters	
Size	
Torus OD	26.2 m
Torus height	14.4 m
Double wall thickness	0.38–0.78 m
Shell thickness	40–60 mm
Rib thickness	30–60 mm
Weight	
Vessel and port structures (excl. shielding)	∼5800 t
Shielding	∼4000 t
Cooling	
Heat removal capacity	3 MW
Coolant fluid	Water
Total flow rate (normal op.)	80 kg/s
Total flow rate (fully developed natural convection)	∼130 kg/s
Materials	
Main vessel	SS 316 L(N)-IG
Primary vessel shielding (with 2% boron)	SS 30467
Ferromagnetic shielding	SS 430

The VV components need to be designed and manufactured consistently with the RCC-MR code [42].

3.1. VV Components

3.1.1. Main Vessel

The main vessel consists of inner and outer shells, ribs, shield structures, splice plates, shielding structures for field joints, and mechanical structures on the inner and outer shells to support in-vessel components and to support the vessel weight (see Figure 22).

The double wall structure has stiffening ribs between the shells to give the required mechanical strength and separate the shells. The number of ribs is minimized to simplify the vessel design and to reduce the cost. The basic vessel design is an all-welded structure. The inner and outer shells and stiffening ribs are joined by welding. The shells and ribs form the flow passages for the vessel cooling water. The space between the shells is filled with shielding.
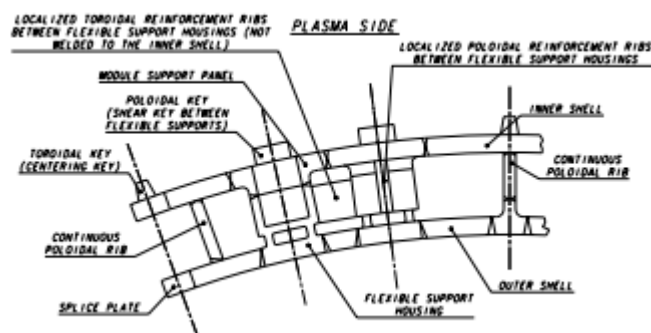
Figure 22: Toroidal Cross Section at Inboard Region *[40]*.

The heavy steel structure of the VV provides a reliable first confinement barrier. Although the VV is a double wall structure, the inner shell serves as the first confinement barrier.

The VV is divided toroidally into 9 sectors joined by field welding using splice plates at the central vertical plane of alternate ports. Each sector includes a full set of port stubs and stub extensions at the toroidal centre of the sector and a set of half port stubs (split on the port centre) on each side. The straight sections of the inboard form a cylinder, and transitions are made to a four-facet per sector design at the top and bottom of this cylindrical section.

The VV is supported by VV gravity supports which minimize the tangential toroidal displacement of VV ports during each pulse.

Each blanket module is attached directly to the VV by a set of four flexible supports located symmetrically with respect to the module centre. The flexible supports are mounted in housings that are recessed into the VV (Figure 22). The direct attachment of the modules to the VV produces local stresses due to poloidal/radial forces and moments, mainly generated in the modules by plasma disruptions and vertical displacement events (VDEs). To withstand these forces and moments, the vessel shells need to be locally reinforced by toroidal and poloidal ribs in the inboard region where the forces and moments are largest. Poloidal reinforcement ribs are locally connected between the support housings and to the inner shell, while toroidal reinforcement ribs are also used between the housings, but they are not connected to the shells so as not to disturb the water flow.

The blanket cooling manifolds are supported on the VV by brackets that are welded to the vessel inner shell by a set of supports which distribute the reaction force from the manifolds to a wide surface, minimizing the local shear stress in the vessel shell.

In addition to the blanket modules, divertor cassettes are supported by the VV on toroidal rails at the inboard and outboard regions and by radial rails for the three divertor remote handling ports during remote maintenance.
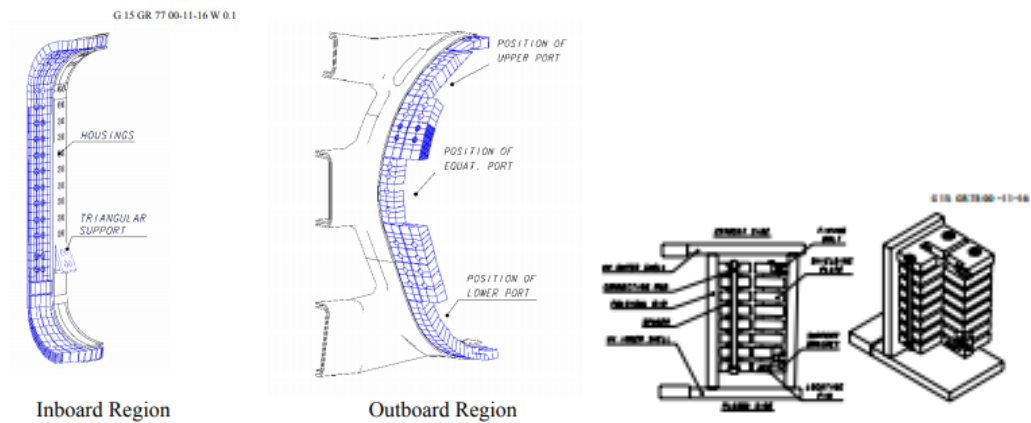
Figure 23: Layout (left) and structures (right) of shields *[40]*.

To provide adequate neutron shielding, the space between the vessel shells is filled, up to 60%, with steel plates (Figure 23).

The vessel is a passive component. There will however be instrumentation to monitor vessel and cooling water temperature, water pressure, local vessel stress/strain, and dynamic movement using thermocouples, pressure gauges, strain gauges and acceleration sensors.

3.1.2. Port Structures

The vacuum vessel has upper, equatorial, and lower port structures that will be used for equipment installation, utility feedthroughs, cryovacuum pumping, and access inside the vessel for maintenance. A typical port structure includes a port stub and a port extension. The port extensions are normally equipped with the closure plates (on the extension end), which provide the primary vacuum boundary. The port stub is welded to the main vessel at the machine assembly station and the port extension is welded to the port stub in the pit. The port extensions are connected to the cryostat by connecting ducts that are a part of the secondary vacuum boundary. The basic port arrangement is shown in **Error! Reference source not found.**.

Figure 24: Port Arrangement *[40]*.

The pipes for the VV water outlet are welded to the port outer surface. The blanket pipes run along the port inner surface and exit the port through chimneys located at the port top before the closure plate.

For the upper ports, the in-port components and the closure plate are integrated into one subassembly. The in-port component, which occupies the space delimited by the blanket pipes, is supported as a cantilever from the end portion of the port extension through the VV closure flange. The vacuum/pressure seal is made with a lip-welded

joint which is incorporated into the bolted flange. The lip seal structure allows repeated cutting/rewelding for the in-port component replacement.
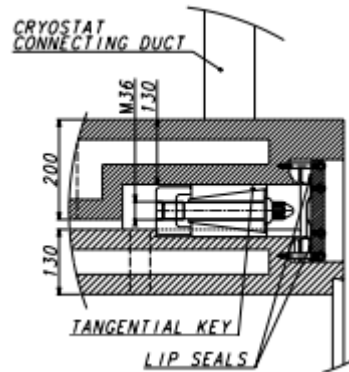
Figure 25: Support Structure of Port Flange *[40]*.

The equatorial ports include regular ports and neutral beam (NB) ports. As in the upper port, the in-port components and the port closure plate are integrated. The NB ports provide an angled access for the neutral beams for plasma heating and current drive. The NB ports are situated in three adjacent sectors of the machine and comprise two heating ports and a combined heating/diagnostic beam port. A massive shield is integrated with the port or main vessel walls to enhance local shielding. Additional but similar structures are required for the plasma diagnostic neutral beam.

The lower ports are inclined downwards and have a trapezoidal cross-section in the area between the TF coils, which transforms to a rectangular cross-section beyond the coils. Each of the three RH/diagnostic ports is equipped with a removable closure plate and has a rectangular-box structure at the end to accommodate diagnostic waveguides. The closure plate of these ports is bolted to the port extension with a lip seal joint as in the upper port.

All lower ports are equipped with pipe stubs for the VV cooling water inlet connections and draining pipes. In addition, the divertor coolant pipe feedthroughs penetrate the port end plate.

3.1.3. Vessel manufacturing

The full chamber is composed by 9 40 degrees sections, called sectors. During manufacturing, each of the sector is achieved by welding together 4 subcomponents, called segments.
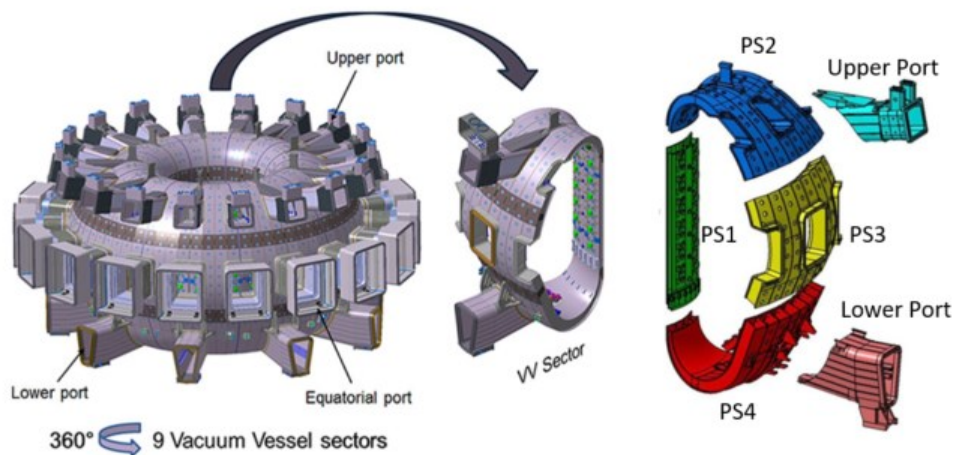
Figure 26: Support Structure of Port Flange *[43]*.

The production of each segment starts from forgings of the Flexible Support Housings (FSHs), port stubs, T-ribs, inner shell plates. Strong jig systems have been applied from the inner shell assembly of the PS manufacturing stage to minimize welding deformation. Narrow gap gas tungsten arc welding (GTAW) was adopted as a basic welding process.

After the inner shell has been consolidated, the In Wall Shielding (IWS) supporting ribs and blocks plates are installed in the interspace. Finally, the outer shell plates are reverse engineered and fitted in between the outer ribs. After being welded together, the final machining of the segment housings and the sector field joint bevels is performed.

The assembly of four poloidal segments into the final D-shaped component, plus the installation of upper and lower port stub extensions, will mark the end of fabrication on the first ITER vacuum vessel sector. The complete sector is finally achieved by repeating the same assembly steps: inner shell and t-rib welding, installation of in wall shielding plates and outer shell welding. A total of 20 welding procedure specifications with 44 welding procedure qualification records have been developed for manufacturing of the ITER VV sector and port.
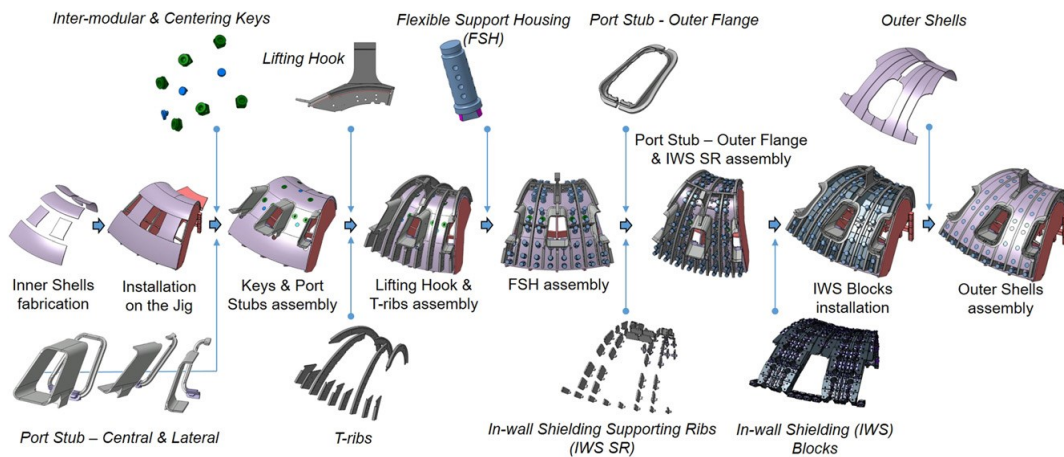
Figure 27: VV segment manufacturing *[44]*.

4 Reconstruction

An exercise of reconstruction of non-ideal Skin surface model has been developed on the TF WP and the VV IS.

The reconstruction process workflow developed for the scope can be divided in the following steps:

- Acquisition of as-built data;
- Data preparation;
- Morphing;
- CAD reconstruction.

Two are the inputs of the reconstruction process. On one side, the manufactured surfaces data, which can be acquired through several metrology techniques, as described in section 4.1. The imported point cloud, in the form of XYZ coordinates of the surface points, needs to be triangulated in order to generate the target STL for the RBF morphing algorithm. On the other side is the object of the geometry update, the nominal CAD model. Each of the reference surfaces has to be isolated from the source model and associated to the corresponding point cloud to preserve the topology in the following steps of the reconstruction. From each single surface, a mesh is generated in order to feed the RBF morphing algorithm with the source points. The processing of the input data is described in section 4.2. Through morphing, the distance between the mesh of each surface of the reference CAD model and its corresponding portion of the target STL is optimized, as described in section 4.3. The output morphed mesh is finally the object of the NURBS patching (section 4.4). The initial topology is recovered from the association performed during the data preparation, while the updated geometry tackles the as-built data.

This workflow has been developed in particular for its capability to produce an updated shape maintaining the initial CAD topology and the possibility to generate a displacements field without a reference geometry of the morphing algorithm.
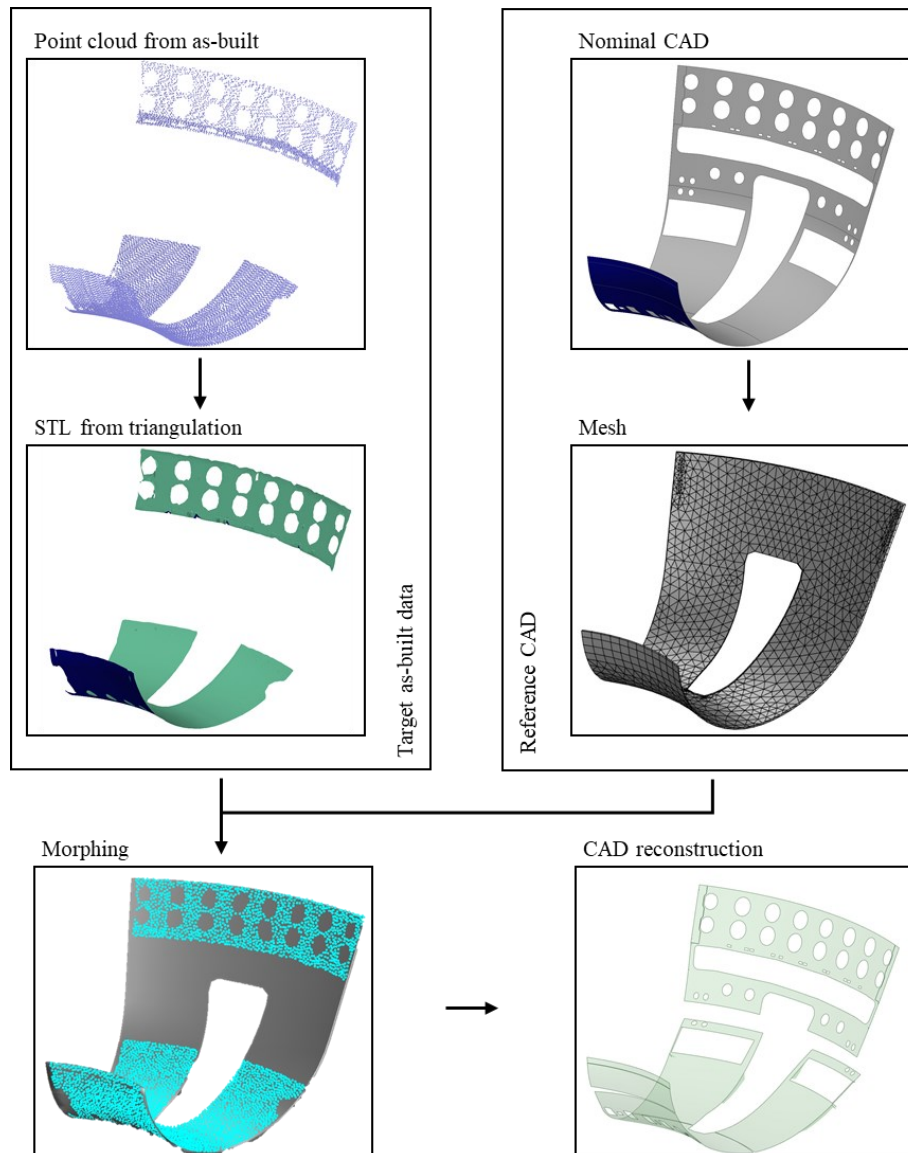
Figure 28: Reconstruction workflow

4.1. As-built data acquisition

The process of update of the nominal geometry on manufactured shapes start from the acquisition of the data. To accomplish it, high quality metrological techniques are to be considered as fundamental tools. Blue light scans, photogrammetry and contact-based measurement systems are typically used to verify the deviation of the real product from the reference CAD geometry. A brief description of the instrument commonly used is given in the first section of this chapter.

4.1.1. CMM

CMM (Coordinates Measuring Machines) are well established instruments in the industry for the high accuracy, automated measurement of size, shapes, position and orientation of manufactured items.

A granite base table, a moving bridge and a measuring head are the components which determine the measurement volume of the machine. The single point measurement is acquired when the measuring head probe contacts the item surface   to be measured. Readers moving together with the bridge and the measuring head along the three axes register values of the corresponding fixed scale with microscopic fine line graduations. The translation of the readings gives the 3d coordinates of the measured point.

Figure 29: CMM machine [Retrieved on 21 Jul 2022 on www.hexagonmi.com]

For a CMM, the accuracy is in the order of microns. Being the system highly relying on contact, it is very sensible to temperature gradients. The different rates of the components thermal expansion, made in aluminum, steel and granite, might lead to bending and twists which cannot be controlled and affect the accuracy of the machine. A strict temperature control is often required in the measuring environment, which can only be anchieved in laboratories.

4.1.2. ARM

ARM is a type of Portable Coordinate Measuring Machine (PCMM) designed to overcome the limits of limited volume and controlled environment of traditional bridge CMMs, fulfilling an area of metrology that they could not address: measuring the part on the shopfloor itself, sometimes even in-process.
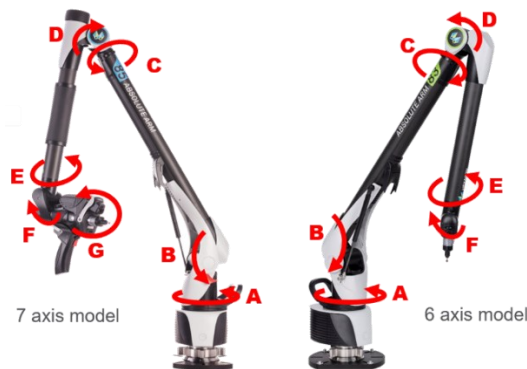
Figure 30: ARM machine [Retrieved on 21 Jul 2022 on www.hexagonmi.com]

The ARM works by using the relative rotation of the 6 (or 7) individual encoders to determine the location and the direction of the hard probe. The point coordinates can be retrieved by combining the angular information of each encoder with the length of each segment attached to it, as shown in the simple example below for a three-link planar manipulator:
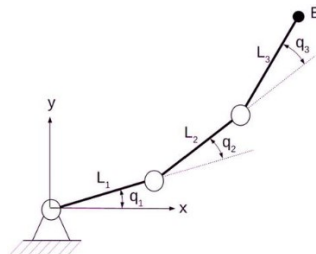
Figure 31: 3D planar manipulator cinematic scheme

$$\begin{cases} x_E = L_1 \cos q_1 + L_2 \cos(q_1 + q_2) + L_3 \cos(q_1 + q_2 + q_3) \\ y_E = L_1 \sin q_1 + L_2 \sin(q_1 + q_2) + L_3 \sin(q_1 + q_2 + q_3) \end{cases} \tag{3}$$

4.1.3.   Laser Tracker and Scanner

A laser tracker is a three-dimensional, optical PCMM that uses angle encoders and a laser beam to determine a target's point coordinates. The laser tracker body follows a retroreflector (SMR), a calibrated sphere with a mirror surface inside which, no matter which angle the laser light is received, it returns the light in the direction in which it came. light by rotating in the horizontal and vertical directions.

The sensor head is the component in which the optics is. It gives the reference center coordinate system for the measurements.
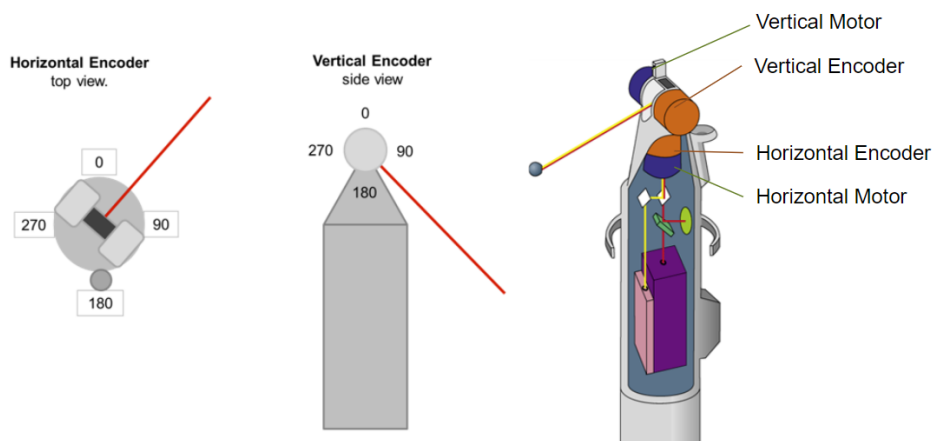
Figure 32: Laser tracker components

The laser tracker calculates the center coordinates (XYZ) of the SMR from the distance (D) and angle information from the horizontal (H) and vertical (V) two-axis rotary encoders. The distance is evaluated by the use of laser technology. Two are the methodologies developed for the scope:

- IFM (Laser Interferometer): it evaluates the relative distance by combining the wavelengths of the exiting and returning laser beams.
    o   Instant measurements, perfect for dynamic measurements
    o   Only relative positions can be evaluated

Figure 33: Laser Interferometer [Retrieved on 21 Jul 2022 on www.hexagonmi.com]

- ADM (Absolute Distance Meter): by integrating the wavelength measurements with information about the modulation frequency of the polarized light, the absolute minimums of the waveform can be found.
  - Absolute position can be measured without setting a zero of the system
  - The integration process requires a stable point, not suitable for dynamic measurements
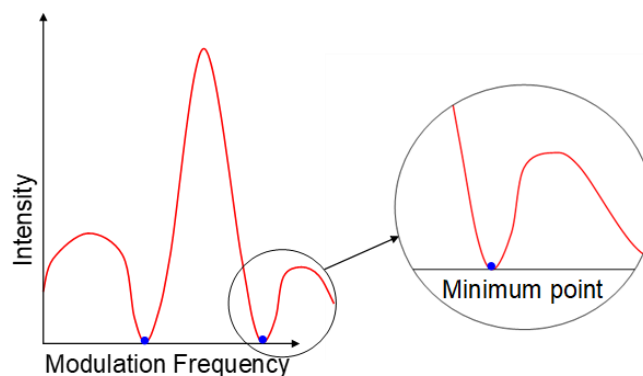
Figure 34: Absolute Distance Meter [Retrieved on 21 Jul 2022 on www.hexagonmi.com]

These two technologies can be found integrated together in the latest Laser Tracker models, having dynamic measures of absolute distances. The name attributed to the technology is AIFM (Absolute Laser Interferometer). Errors in the measures of the ADM distance due to the movement of the reflectors are corrected instantly by the information provided by the IFM.

Figure 35: Absolute Laser Interferometer [Retrieved on 21 Jul 2022 on www.hexagonmi.com]

For laser tracker systems, the accuracy of the measurement (how much the tracker is close to the true value) is usually specified in microns. A typical accuracy statement for a tracker is composed by an initial uncertainty, which is fixed, and a combined angle and distance scale error uncertainty, which depends on the distance:

Measured value $\pm$ (15 μm + 6 μm/m) $\hspace{3cm}$ (4)

4.1.4.   Photogrammetry

Photogrammetry, as its name implies, is a 3-dimensional coordinate measuring technique that uses photographs as the fundamental medium for metrology (or measurement).

Every photogrammetry system measures special targets made of a thin (0.15mm thick), flat, retro-reflective material. Retroreflectors reflect light very efficiently back to the light source. For example, they are typically 100 to 1000 times more efficient at returning light than a conventional white target. A low-power flash located on the camera is used to illuminate the targets. The resulting target images are very bright and easy to find and measure. In addition, because the targets are illuminated completely by the flash, the target exposure is independent of the ambient illumination. Pictures can be taken in bright light or total darkness and the target exposure will be the same.

Unilluminated retro target   **Illuminated retro target**
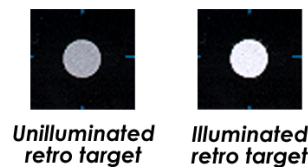
Figure 36: Retroreflectors [Retrieved on 21 Jul 2022 on www.geodetic.com]

The fundamental principles used by photogrammetry are triangulation and resection.

Triangulation is the procedure used to combine points taken by multiple pictures into 3D coordinates locations. By taking photographs from at least two different locations, so-called "lines of sight" can be developed from each camera to retro-reflective targets on the object. If the camera location and aiming direction are known, the lines can be mathematically intersected to produce the XYZ coordinates of each targeted point.

Resection is the procedure used to determine the final position and aiming (called the orientation) of the camera when a picture is taken. Typically, all the points that are seen and known in XYZ in the image are used to determine this orientation. If the

XYZ coordinates of the points on the object are known, the camera's orientation can be computed. It is important to realize that both the position and aiming direction of the camera are needed. It is not sufficient to know only the camera's position since the camera could be located in the same place but be aimed in any direction. Consequently, we must know the camera's position which is defined by three coordinates, and where it is aimed which is defined by three angles. Thus, although three values are needed to define a target point (three coordinates for its position), six values to define a picture are needed (three coordinates for position, and three angles for the aiming direction).
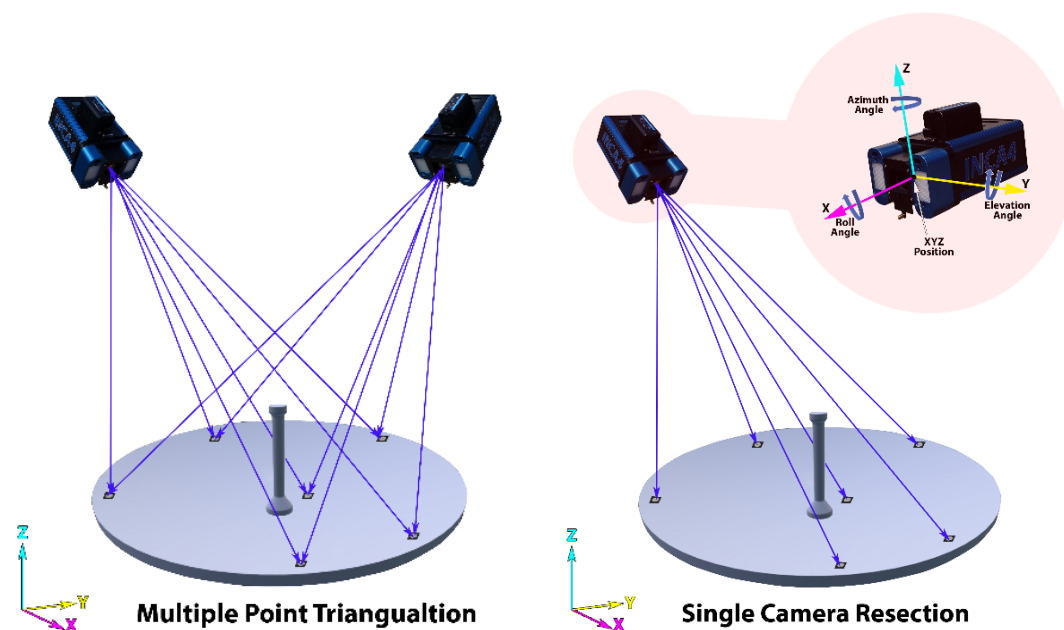
**Figure 37**: Triangulation and Resection [Retrieved on 21 Jul 2022 on www.geodetic.com]

4.1.5. 3D volumetric scan

3D scanners are a non-contact 3D technology developed to have a fast acquisition of a huge amount of point data. They are particularly adequate for scanning of highly detailed organic surfaces, fragile objects that cannot be touched physically by a measurement device or scanning of big volumes. They can be divided in the following sub-categories:

- PCMM scanners
- Structured light 3D scanners
- Laser scanners

4.1.5.1. PCMM scanners

PCMM scanners combines the capability of registration of a laser tracker or ARM with scanning heads for the acquisition of multiple points measurements. In this section, the functionality of a laser tracker combined with a scanning head will be detailed.
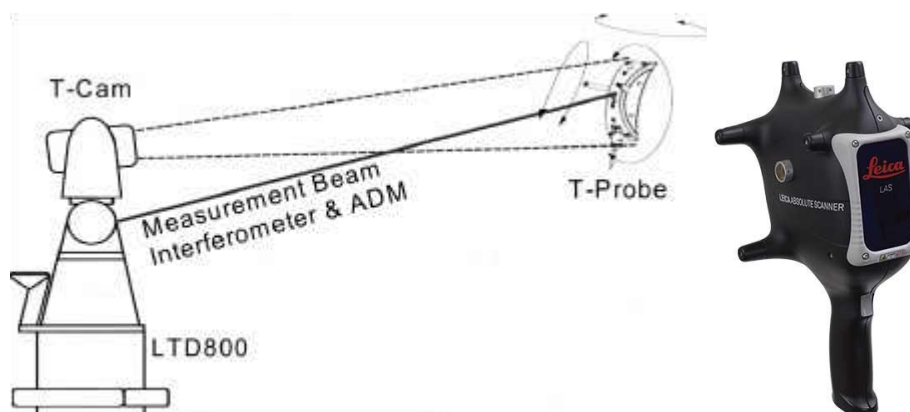
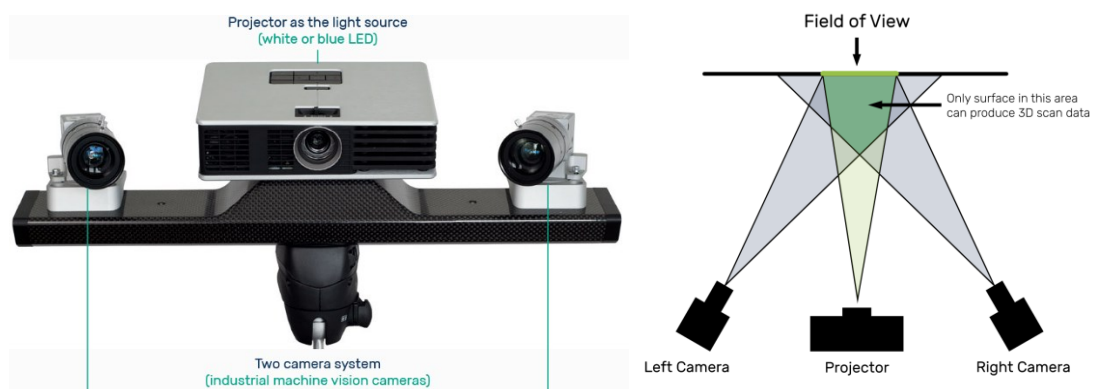**Figure 38:** PCMM scanner principle [Retrieved on 21 Jul 2022 on www.hexagonmi.com]

The scanner head is equipped with a line laser source which emits the beam line and sensors to combine the information on the wavelength in order to retrieve the distance

covered by the beam. A prism, similar to the one equipped on retroreflective targets, is targeted by the laser tracker beam and returns the information of the distance of the laser head to the laser tracker. In addition to this, the position of Infrared Pulse Antennas on every side of the scanner head is recorded by tracker built-it camera, allowing the definition of the head "spatial orientation".

4.1.5.2. Structured light 3D scanners

A structured-light 3D scanner specifically uses projected light patterns (either white light or blue light) in combination with a camera system to produce a 3D scan.

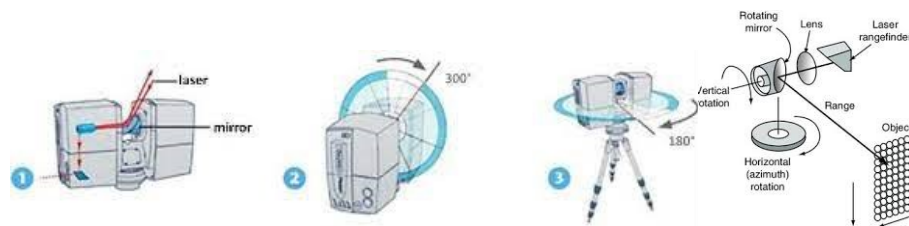**Figure 39:** PCMM scanner principle [Retrieved on 21 Jul 2022 on www.hexagonmi.com]

The light source from the scan head projects a series of parallel black and white patterns onto the scan target. When light projects onto the object's surface, the patterns become distorted. The images captured by the cameras can be triangulated and combined with the information of the distance and angle of the cameras to reconstruct the 3D scene.

4.1.5.3. Laser scanners

Laser scanner technology is derived from the laser trackers. They are used mainly in design and construction projects and topographic surveys due to their capability to quickly capture millions of points around the scene.

The fundamentals of a laser scanner are very similar to the ones of a laser tracker.

The laser scanner emits a rapidly pulsing or continuous laser beam. As it emits the scanner head automatically rotates around its vertical axis and a spinning or oscillating mirror also projects the beam around the horizontal axis. This combined movement allows the beam to cover a spherical area.

Figure 40: PCMM scanner principle [Retrieved on 21 Jul 2022 on www.hexagonmi.com]

As per the laser tracker, an interferometer evaluates the distance by combining the wavelength of the exiting and returning beam line.

The information of the distance, combined with the horizontal angle of the scanner head and the vertical angle of the mirror, can be translated in 3d coordinates. The result of the scan is a set of 3d coordinates measurements, a 3d representation of the scene called point cloud. Coloured scans can also be obtained by combining the point cloud information with pictures collected during the scan by the built-in camera.

Multiple scans of different scenes can be aligned together by usage of scan targets or markers placed around the site.

4.2. Data preparation

The outcome of the scan is a point cloud. The component surfaces are usually represented by the coordinates XYZ of each point retrieved by the instrument. An association algorithm organizes the scan data on the basis of the nominal CAD topology. The algorithm filters the data by setting two thresholds T_n and T_e, representing respectively the distance from the CAD surface and edge.
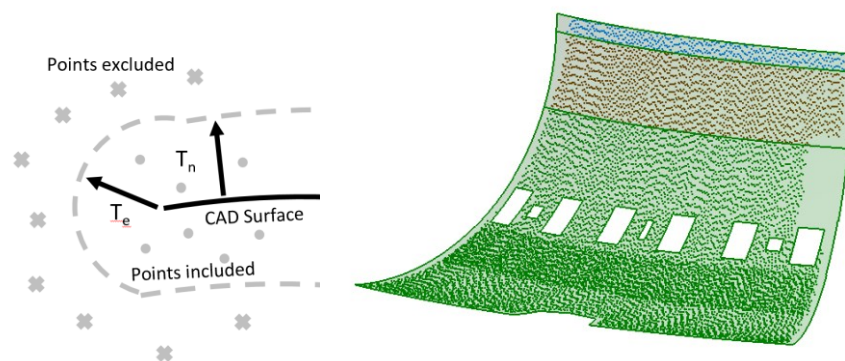
Figure 41: Association of scan data to nominal CAD surfaces

From the organized point clouds, the corresponding STL is created by Delaunay triangulation algorithm. For 3D points sets, triangulation is achieved by connecting points to their neighbours to form edges that form triangulated or polygonal shapes. Widely used by RE and meshing software, Delaunay triangulation is a technique which maximizes the minimum angle of triangles generated for a given set of points.
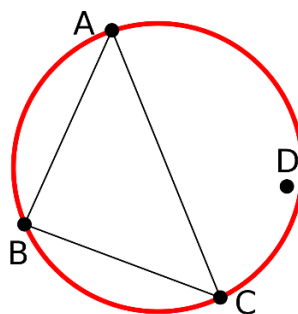
Figure 42: Evaluation of circumscribed circle

The optimization is carried out by constructing triangles from every combination of point triplets in the set. If the circumscribed circle of the triangle includes additional points in the set, it is excluded from the triangulation. In a 2D representation, this condition is evaluated by computing the determinant of the following matrix composed by the coordinates of four points in counterclockwise order:

$$\begin{vmatrix} A_x & A_y & A_x{}^2 + A_y{}^2 & 1 \\ B_x & B_y & B_x{}^2 + B_y{}^2 & 1 \\ C_x & C_y & C_x{}^2 + C_y{}^2 & 1 \\ D_x & D_y & D_x{}^2 + D_y{}^2 & 1 \end{vmatrix} > 0 \tag{5}$$

If the determinant is positive, the triangle has to be excluded from the triangulation.
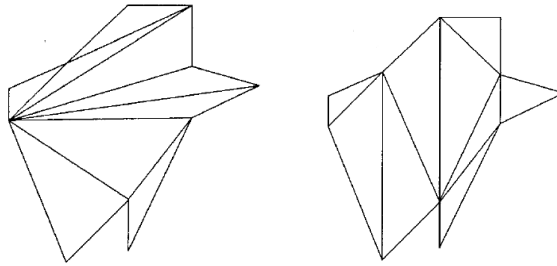
Figure 43: Triangulation by otectomy (left) and Delaunay triangulation (right)

From the nominal CAD surfaces a mesh is generated through meshing algorithms. Differently from FEA applications, the impact of the mesh quality on the result of the reconstruction is limited to the surface distribution of the mesh nodes, which will be a parameter of the B-spline surface fitting described in section 4.4. In order to obtain a homogeneous grid of nodes and to guarantee a minimum number of points over the surfaces with different extensions, the Delaunay triangulation is combined with adaptive sizing algorithms. As result, the surface mesh will produce the source points for the generation of the displacement fields in the morphing.

4.3. Morphing

The input STL is the target of the morphing action. For the application, a cubic spline function $\varphi(r) = |r|^3$ is substituted in equation (1), giving the following formula:

$$s(x) = \sum_{i=1}^{N} \gamma_i \left(\sqrt{\left(x - x_{s_i}\right)^2 + \left(y - y_{s_i}\right)^2 + \left(z - z_{s_i}\right)^2} \right)^3 + h(x) \qquad (6)$$

On-surface and off-surface points' distribution contributes to the construction of the function s(x), representing the interpolating, implicit zero iso-surface. Respectively at the surface inward and outward, two off-surface points are generated for every on-surface point, at a prescribed distance along the normal direction. Offset distance should be small enough to prevent off-surface points from clashing in regions of the surface characterized by small radiuses of curvature. The projection onto the implicit surface is carried out by Newton's iteration method. The gradient of the function s(x) is:

$$\nabla s(x) = \left\{ \frac{\partial s(x)}{\partial x} \quad \frac{\partial s(x)}{\partial y} \quad \frac{\partial s(x)}{\partial z} \right\}^T \qquad (7)$$

Where:

$$\frac{\partial s(x)}{\partial x} = 3 \sum_{i=1}^{N} \gamma_i \left(x - x_{s_i}\right) \sqrt{\left(x - x_{s_i}\right)^2 + \left(y - y_{s_i}\right)^2 + \left(z - z_{s_i}\right)^2} + \beta_1$$

$$\frac{\partial s(x)}{\partial y} = 3 \sum_{i=1}^{N} \gamma_i \left(y - y_{s_i}\right) \sqrt{\left(x - x_{s_i}\right)^2 + \left(y - y_{s_i}\right)^2 + \left(z - z_{s_i}\right)^2} + \beta_2 \qquad (8)$$

$$\frac{\partial s(x)}{\partial z} = 3 \sum_{i=1}^{N} \gamma_i \left(z - z_{s_i}\right) \sqrt{\left(x - x_{s_i}\right)^2 + \left(y - y_{s_i}\right)^2 + \left(z - z_{s_i}\right)^2} + \beta_3$$

The projection of a point x onto the implicit surface can then be calculated iteratively by:

$$x_{k+1} = x_k + \frac{s(x_k)}{\|\nabla s(x_k)\|^2} \nabla s(x_k) \qquad (9)$$

The above iteration runs until $\|x_{k+1} - x_k\|$ is less than a given tolerance.

4.4. CAD reconstruction

Over each of the organized faces of the morphed mesh a tensor product B-spline patch is defined.

In the most general setting, a B-spline surface $s_f(u, v)$ is defined as a network of tensor product B-spline surface patches:

$$s_f(u, v) = \sum_{r=0}^{n_f} \sum_{s=0}^{m_f} d_{r,s}^f N_{r,k_f}(u) N_{s,l_f}(v) \qquad (9)$$

Here $d_{r,s}^f$ denote the control points, $N_{r,k_f}(u)$ are the univariate B-spline basis functions of order k_f in the u-direction, defined over the knot sequences $U_f = (u_0, u_1, \ldots, u_{n_f+k_f})$ and $N_{s,l_f}(v)$ are defined analogously over the knot vectors V_f in the v-direction.

In surface reconstruction the objective is to find the control points $d_{r,s}^f$ of all patches s_f such that the distance of the mesh points p_i to the surface S is minimized. More precisely, the following distance functional is minimized:

$$E_{dist}(S) = \sum_{i=1}^{N} d^2(p_i, S) \qquad (10)$$

Iterative methods have been developed to solve this type of nested minimization problem in the context of B-spline surface fitting. In these methods, each iteration consists of two steps:

- Fitting step: For fixed parametrizations t_i, the optimal control points $d_{r,s}^f$ are found by solving a linear least-squares problem.
- Parameter correction step: For fixed control points $d_{r,s}^f$, optimal parametrizations t_i are found by projecting the points onto S.

The method ensures the convergence of the results after few iterations.

The full morphed CAD model can be reconstructed by automating the optimization of B-spline patching. A tool recovering the initial CAD topology on the morphed mesh and fitting the B-spline patch has been developed.

Mesh morphed

Retrieval of CAD topology

Fitted B-spline patches
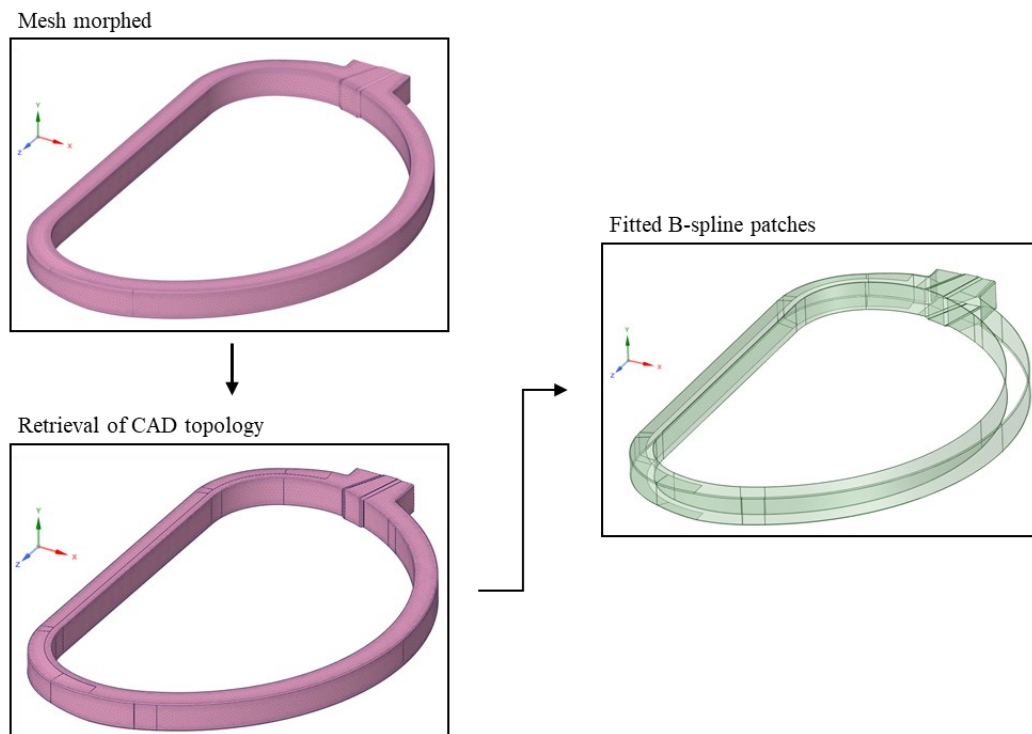
Figure 44: Automation tool

4.5.   Reconstruction of the WP

The reconstruction workflow has been tested during the manufacturing of the TF WP.

Before the delivery of the WP, a series of final tests are carried out, including dimensional checks. A full 3D scan with PCMM scanning technology is performed at the end of the production, in order to certify the external surface quality, the final dimensions of the superconductor and the interfaces in the terminal area.

With regards to the acquisition time and the component requirements in terms of quality of the measurements, three types of sampling areas are present in the final scan, each of them characterised by a different resolution and measurement uncertainty:

Table 4: Sampling areas resolution and related uncertainty

Resolution [mm]	Total uncertainty at 2σ confidence interval [mm]
4	0.224
1	0.210
0.4	0.197
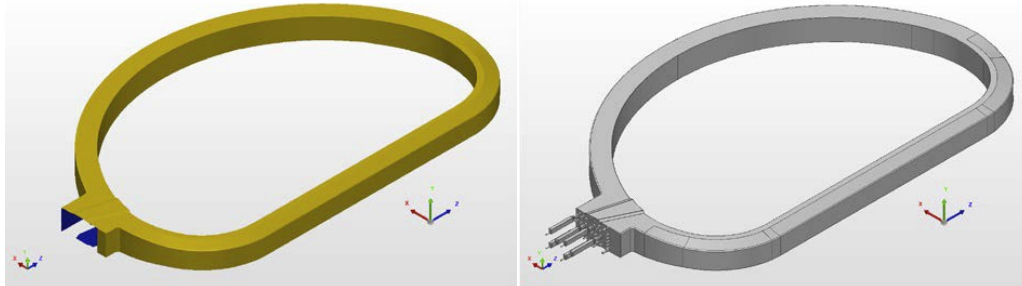
**Figure 45**: WP scan data (left) and baseline CAD model (right).

As shown in Figure 46, the optimization of the DP stacking process led to the production of slimmer WPs. The deviations of the scan data from the nominal CAD show this phenomenon, with values of 2.5-4 mm on top and bottom surfaces in the Y

direction, along which the DPs are stacked, while on the remaining faces smaller values are reported.

Table 5: Deviation of measured data from CAD nominal surfaces

CAD nominal deviations	
AvDev	-1.566
StdDev	1.425
Pts within +/-(1 * StdDev)	1170173 (68.707%)
Pts within +/-(2 * StdDev)	1680289 (98.659%)
Pts within +/-(3 * StdDev)	1702173 (99.944%)
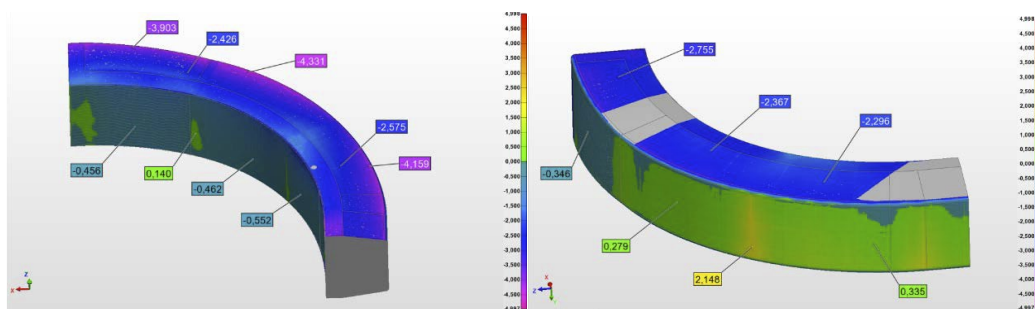
Figure 46: Deviations of the scan data from the nominal CAD surfaces

A portion of the top end of the WP straight leg has been used in the test (see Figure 47). The section transition and the complexity of the CAD surfaces make this portion a representative sample of the overall problem.
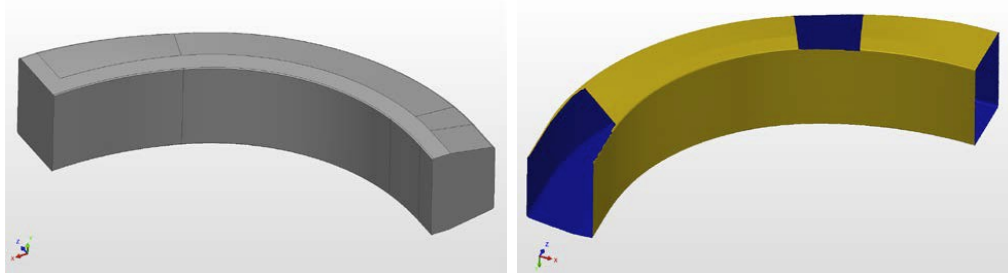
Figure 47: Model sample CAD geometry (left) and Missing scan areas.(right).

Due to the supporting configuration of the WP during the scan acquisition, some areas of the STL model do not present point data. To ease the solution of the RBF system in the morphing algorithm, fictitious points have been included in the model, respecting the curvature of the surrounding areas (see Figure 47).

The mesh is generated from the CAD initial geometry to obtain source points for the morphing routine. Nodes are arranged in sets corresponding to their respective CAD surfaces, which will be used for the update CAD generation. Overall nodal spacing is 50 mm, with refined zones (2 mm spacing) in the fillet areas (see Figure 48)
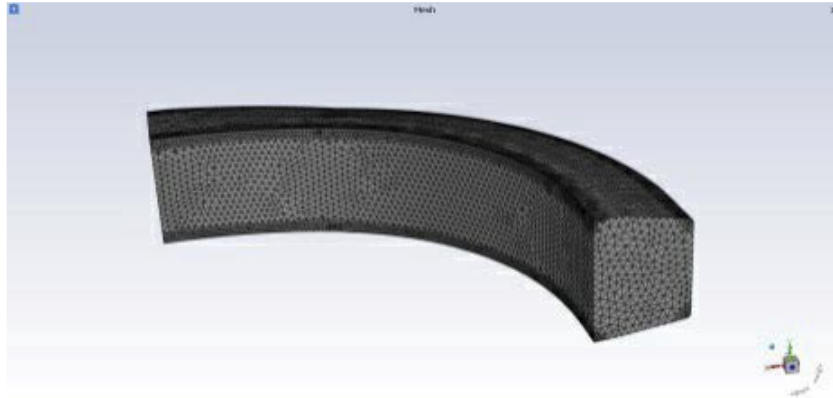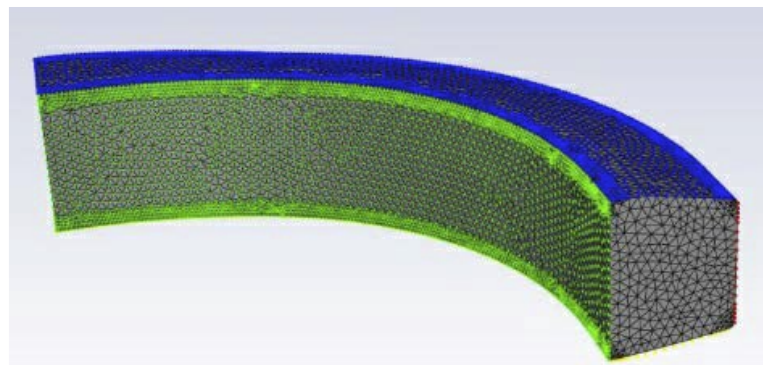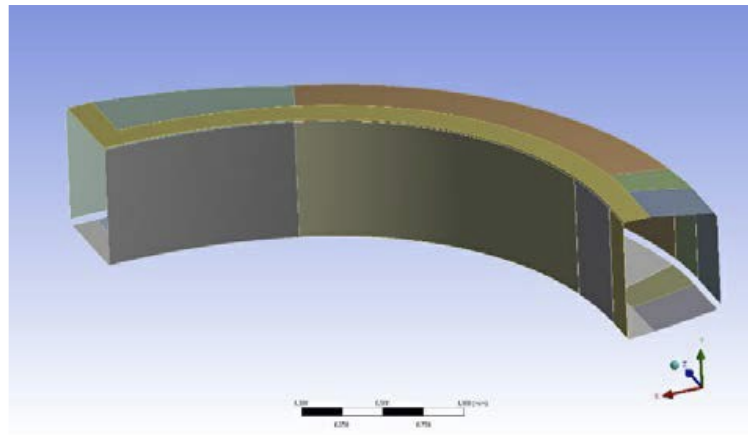

Figure 48: Mesh detail.

The above-mentioned point cloud and the STL scan are the input data for the RBF algorithm generates the displacement field and applies it to the CAD point data, producing the morphed mesh (see Figure 49).

Figure 49: Source point sets for the morphing

As final step, in Figure 50 the result of the reconstruction method is shown.

Figure 50: Reconstructed surfaces.

To highlight the differences from the initial configuration, the updated CAD geometry has been compared with the original scan data.

As shown in Figure 51, the resulting geometry adapted to the target scan data with high accuracy. Updated surfaces show a wavelike behaviour, with differences from the target that vary from 0.05 mm to 0.5 mm, with a standard deviation of 0.2 mm.
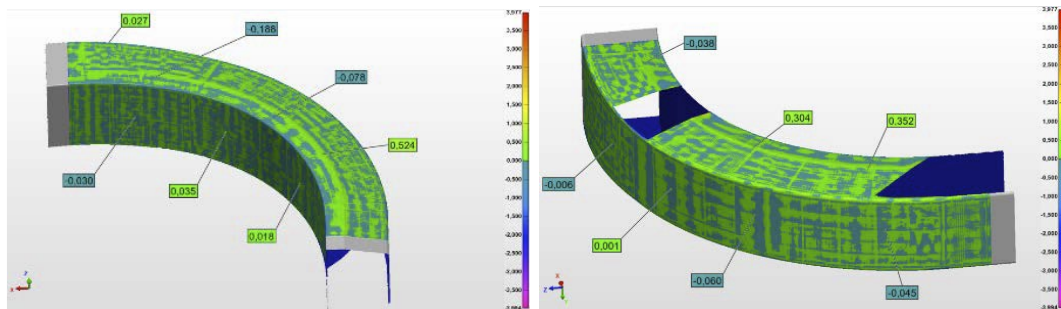
Figure 51: Deviations of the scan data from the updated CAD surfaces.

To give an insight into the performances of the methodology, a comparison with a commercial RE software is proposed in Table 6. The software makes usage of NURBS patching method (see Figure 52) to reconstruct the CAD geometry directly from the scan data.
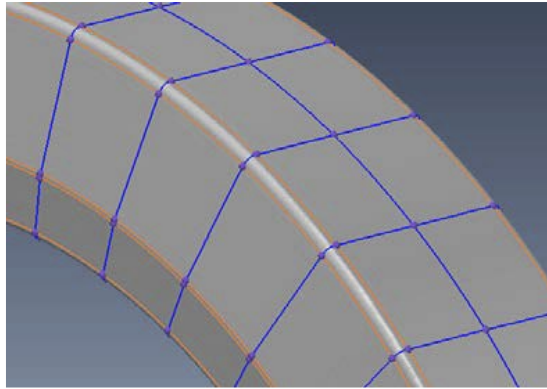
Figure 52: NURBS patches from scan data.

The methods produce comparable results, both in the standard deviation and in the shape of the Gaussian distribution.

It has to be remarked that, even if the NURBS patching method produce slightly better results than the morphing method, the process generates a different surface topology with respect to the initial configuration.

Table 6: Methods comparison.

Method	CAD morphing	NURBS patching
StdDev	0.221	0.087
Pts within +/-(1 * StdDev)	1468351 (86.409%)	495300 (82.362%)
Pts within +/-(2 * StdDev)	1607505 (94.598%)	571248 (94.991%)
Pts within +/-(3 * StdDev)	1658204 (97.581%)	590666 (98.220%)

4.6. Reconstruction of the VV IS

Following the same methodology used for the WP case, an exercise of reconstruction of non-ideal Skin surface model has been developed on the VV Inner Shell.

As for the WP case, a full scan of the resulting inner shell surface is performed using PCMM scanning technology. The full scan includes the coordinates of 100k points, with an average point spacing of 10mm.
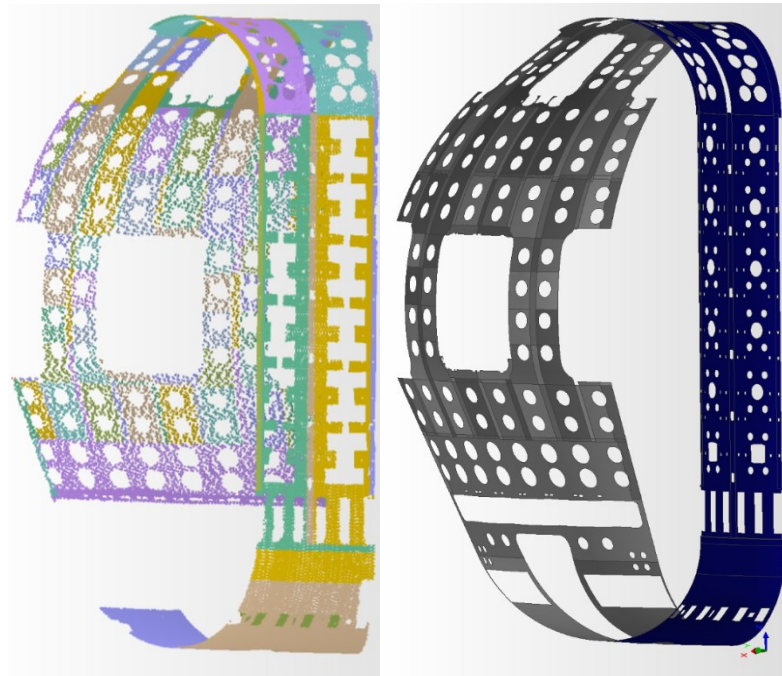
Figure 53: VV scan data (left) and baseline CAD model (right).

With the completion of the inner shell welding between segments, the surface of the vacuum chamber facing the plasma presents a different shape compared to the stage in which the single segments were just aligned on the assembly tool. The welding process induced deformation affected each segment of the vacuum vessel sector differently, depending mainly on the stiffness of the subcomponents and the amount of welding material (and consequent energy) introduced in the process.
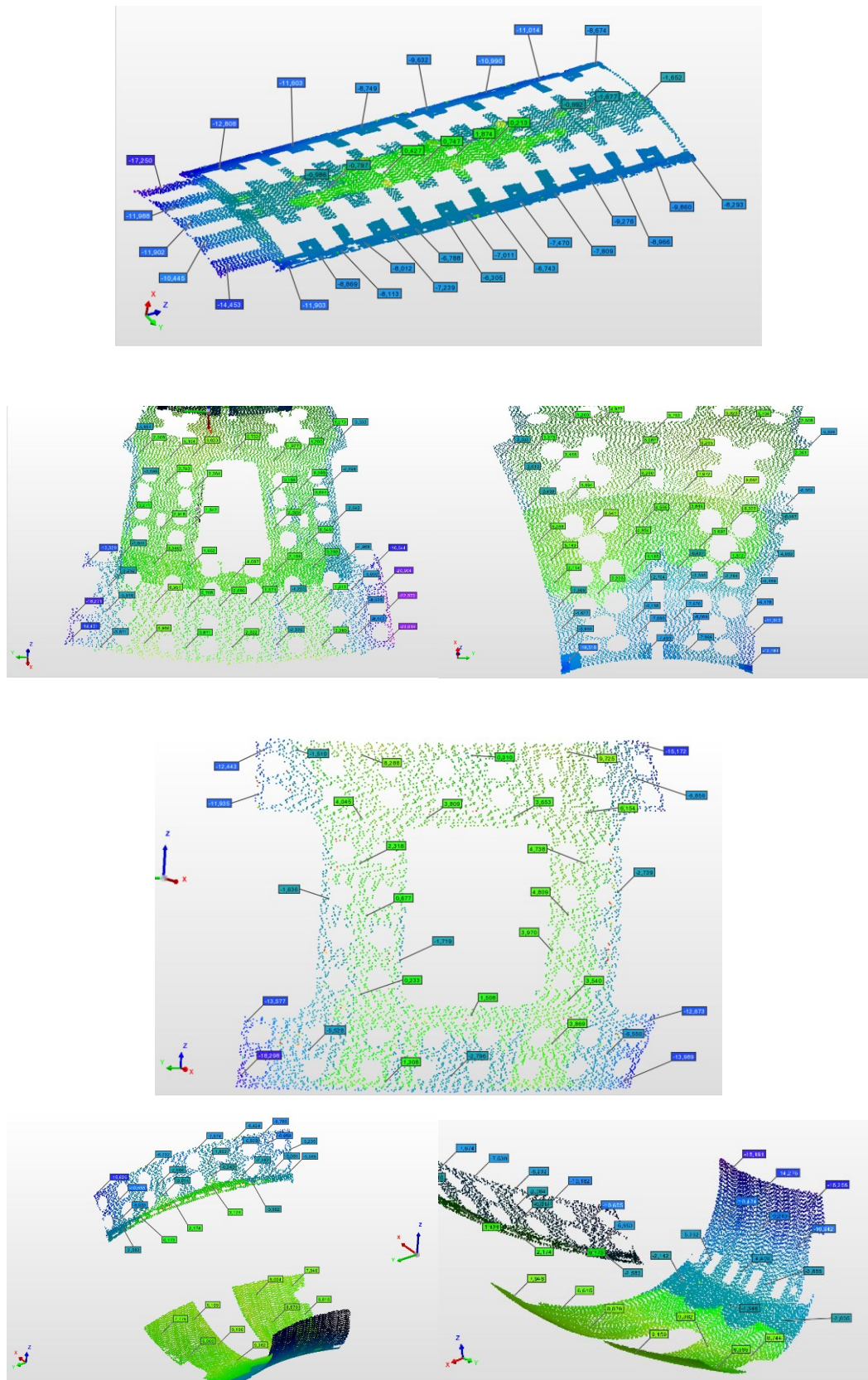
Figure 54: Deviations of the scan data from the nominal CAD surfaces.

Table 7: Deviation of measured data from CAD nominal surfaces

CAD nominal deviations	
AvDev	-1.839
StdDev	6.938
Pts within +/-(1 * StdDev)	65221 (64.437%)
Pts within +/-(2 * StdDev)	98595 (97.410%)
Pts within +/-(3 * StdDev)	101036 (99.821%)

In the exercise, the inner shell CAD nominal surfaces have been extracted from the complete model and defeatured, in order to ease the reconstruction of the CAD model after morphing.
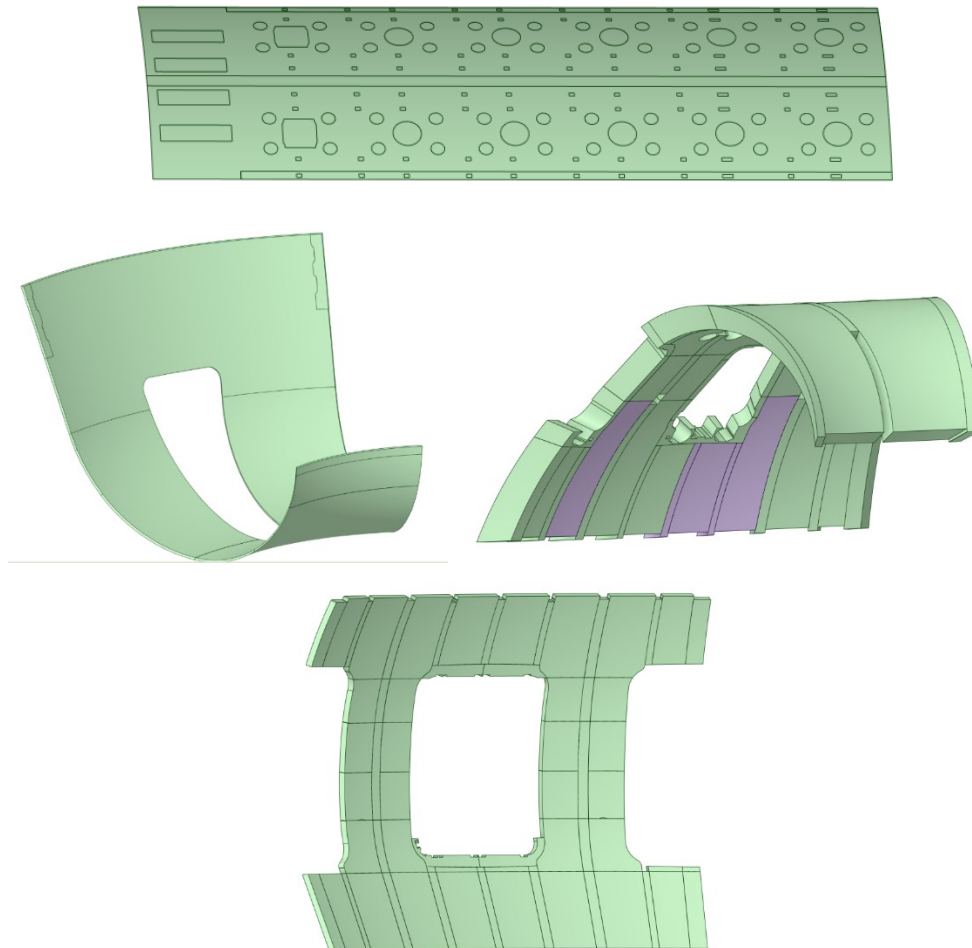
Figure 55: Model sample CAD geometry.

The mesh is generated from the CAD initial geometry to obtain source points for the morphing routine. Nodes are arranged in sets corresponding to their respective CAD surfaces, which will be used for the update CAD generation. Overall nodal spacing is 10 mm.
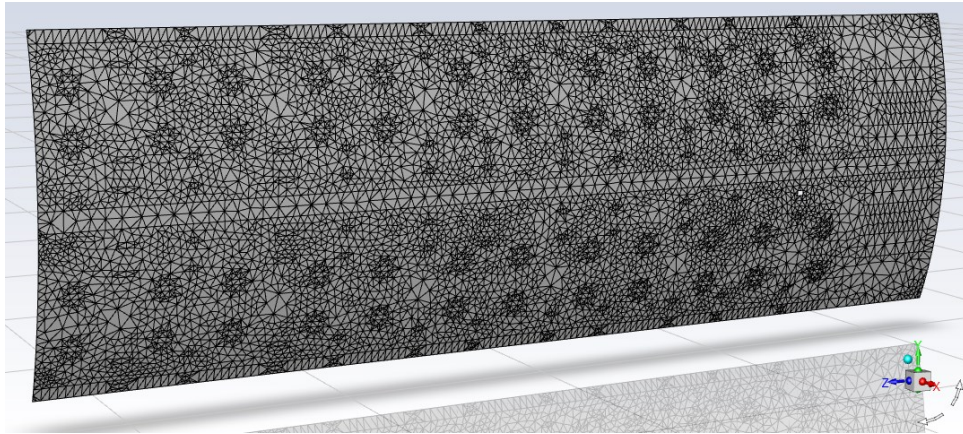
Figure 56 :Mesh detail.

The above-mentioned point cloud and the STL scan are the input data for the RBF algorithm generates the displacement field and applies it to the CAD point data, producing the morphed mesh (see Figure 57).
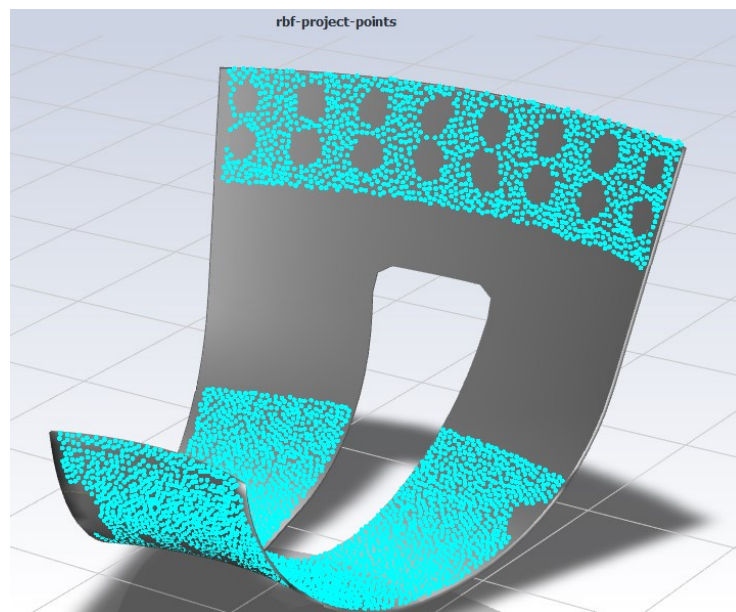
Figure 57: Nodes sets.

As final step, in Figure 58 the result of the reconstruction method is shown.
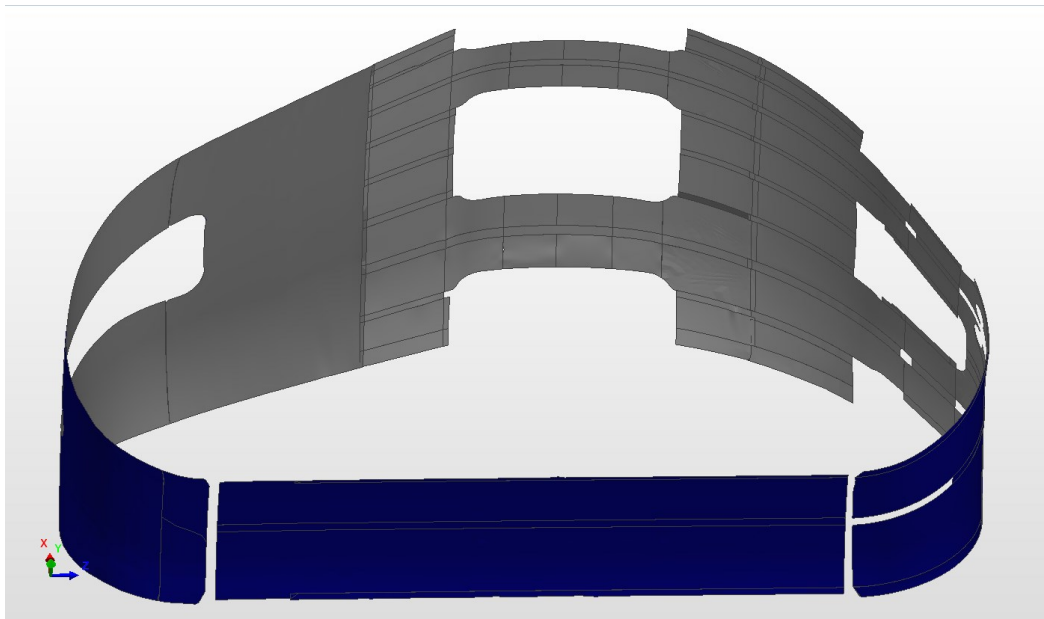
Figure 58: Reconstructed surfaces.

To highlight the differences from the initial configuration, the updated CAD geometry has been compared with the original scan data.

As shown in Figure 59, the resulting geometry adapted to the target scan data with high accuracy. A comparison of deviation with reference to the scan data between original and updated CAD is shown in Table 8.

Table 8: Comparison before and after morphing

	CAD nominal deviations	CAD morphed deviations
AvDev	-1.839	-0.607
StdDev	6.938	1.972
Pts within +/-(1 * StdDev)	65221 (64.437%)	86448 (88.499%)
Pts within +/-(2 * StdDev)	98595 (97.410%)	95065 (97.320%)
Pts within +/-(3 * StdDev)	101036 (99.821%)	96744 (99.039%)

Figure 59: Deviations of the scan data from the updated CAD surfaces.

5   Association

From the initial design stages until the final acceptance of the component, several features have to be monitored. The definition of a Skin Surface model plays an important role in the traceability of the requirements during production.

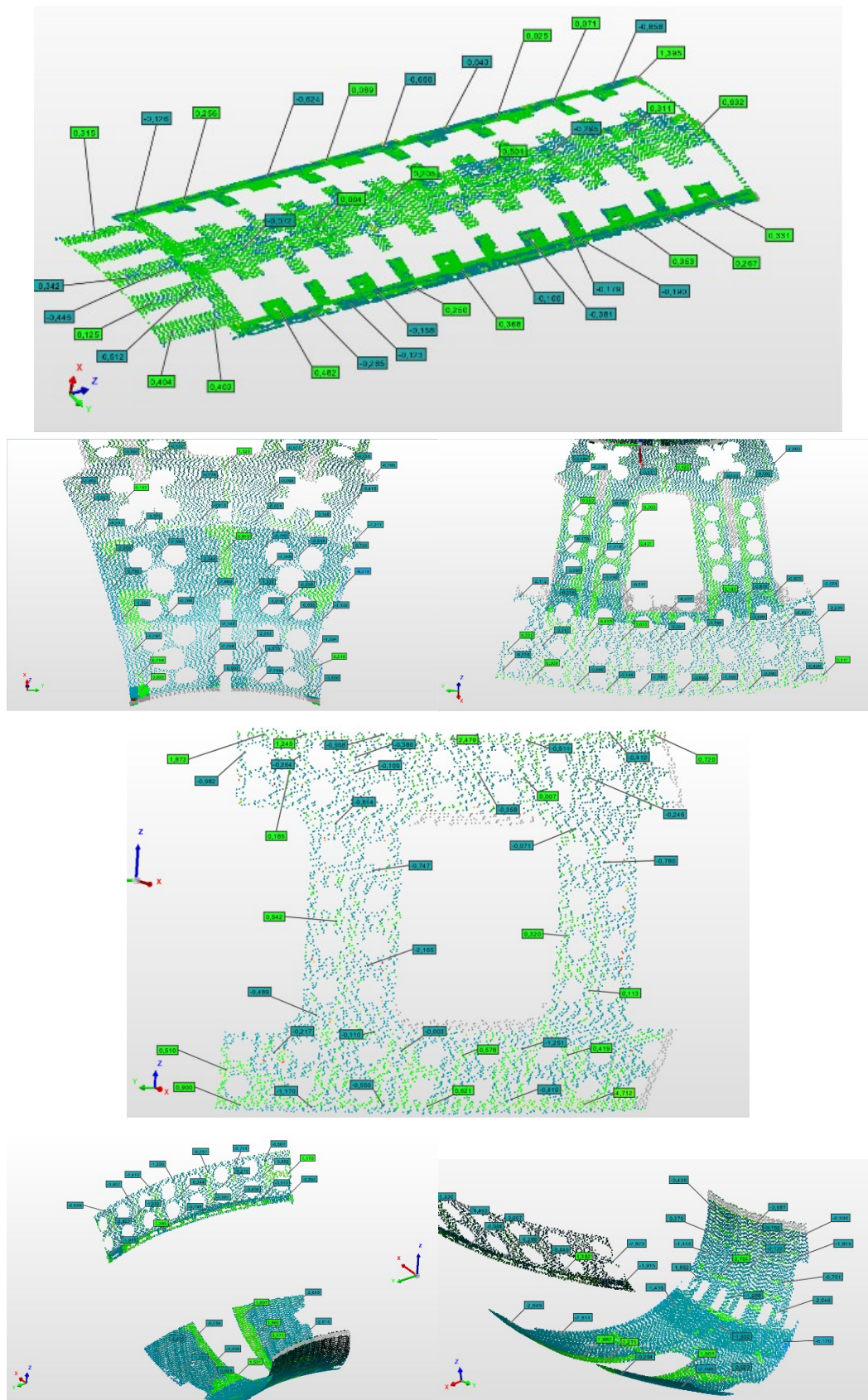In the frame of the ITER project, a special focus has been put on all the actions related to the mitigation of risks linked to features being out of tolerance. In the research scope of this PhD, two techniques adopted for the Skin Model have been deployed in order to investigate possible improvements of the process. Together with the reconstruction of the non-ideal surface model by usage of morphing techniques, the operation of association of measurements to the nominal components has been investigated. In the TF project application, described in section 5.1, the exercise has been performed in the final stages of manufacturing, with the objective of improving the evaluation of conformity of the component by both reducing the time of analysis and by standardizing the measurement process. In the exercise, the alignment of measurements to the nominal model has not been taken into account, being this already fixed by design in the final stages of the manufacturing. However, this element has a paramount importance for the VV project, where in intermediate stages of the manufacturing, far more extended and complex, it can be the key for risk mitigation and the evaluation of conformance of the component. For this scope, the Virtual Fitting method, described in section 5.2, provides the necessary tools for the monitoring and prediction of the actual manufactured shapes deviation from the target nominal model.

5.1. Association in the TF coil

In the design of the TF coil system, the 18 magnets can be grouped in 7 types of different variants, each of them characterized by different features composing the CC interfaces with the tokamak system (PF coils, Central Solenoid). For each of these variants more than 700 checks have to be inspected and evaluated during the last stage of the manufacturing.

Indeed, the preparation of a Skin Model can be of paramount importance in the reduction of time requested for the inspection and verification, reducing the impact on the production schedule. The nominal CAD models of the 7 Coil Cases types have been partitioned, identifying and classifying the features for variant and for required geometrical tolerance.
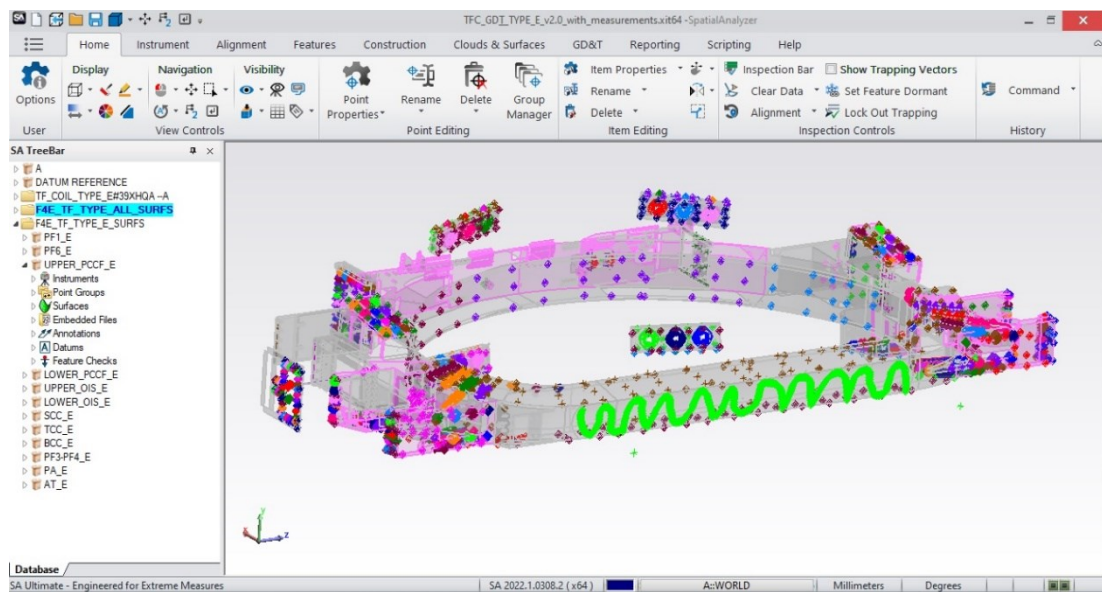
Figure 60: Spatial Analyzer UI

The model has been developed in Spatial Analyzer environment. Spatial Analyzer is the NRK software of reference for dimensional inspections and metrology surveys (Figure 60). It is provided not only with the interface with several different measurement technology available on the market (from 3D scanners to CMMs), but

with modules for the evaluation of process uncertainty and GD&T checks. It makes easy for users to:

- Inspect parts
- Build
- Analyze data
- Report
- Interface with virtually any type of portable metrology instrument
- Automate complex operations to improve measurement and inspection efficiencies.

The Skin Surface model database is tailored for each of the seven TF types as shown in Figure 61. In grey the surfaces in common between variants are represented, while the coloured ones are the surfaces specifics for the variant. The database is composed by several SA files, each one corresponding to a specific interface of the coil.
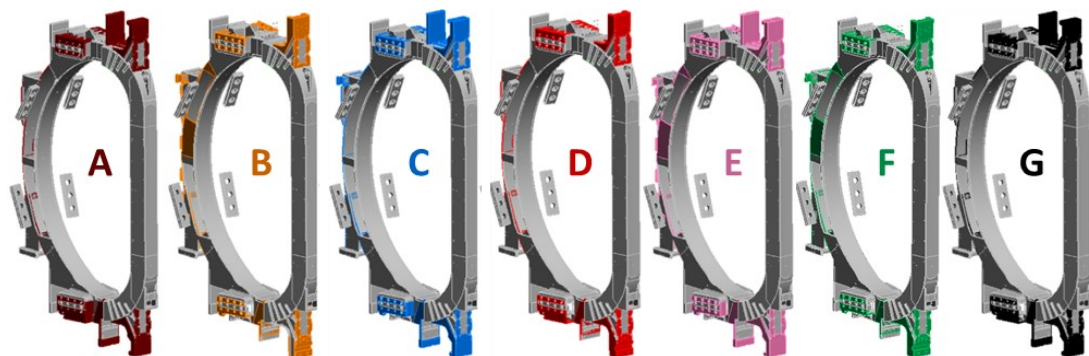
Figure 61: TFCC variants

In the proposed workflow, the metrology operator starts the inspection by selecting the variant corresponding to the component that has to be inspected.

Accessing the database, an automated script helps the operator collecting all the surfaces and checks related to the specific coil type under examination in a single SA file.
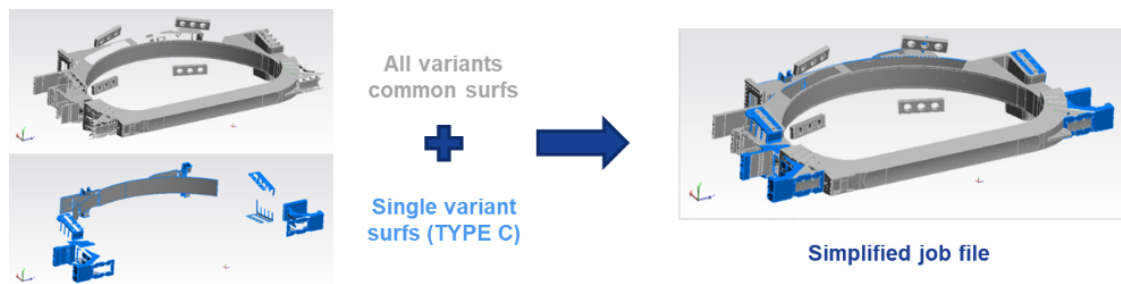
Figure 62: Combination of Skin surfaces

After the measurement campaign has been carried out, the survey data can be imported in the same file, extracted and associated to the corresponding feature, in order for the final postprocessing to be automatically computed.
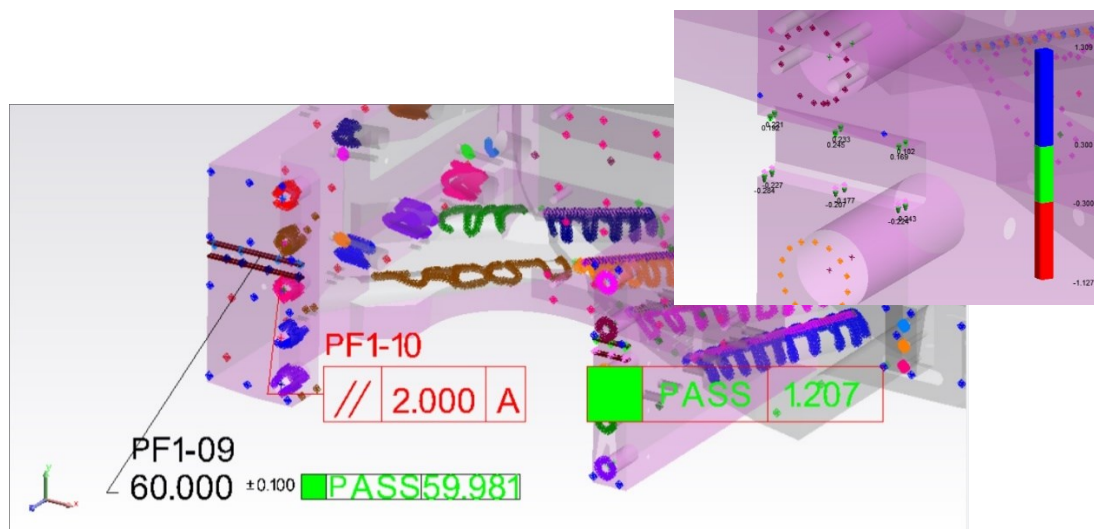
Figure 63: Association of measured data to reference nominal surfaces and results report

The database and the skin model helped in critical stages of the manufacturing, improving the quality and easing the inspection and evaluation of the conformance of the component in the acceptance inspections. Once the extraction, association and collection of nominal surfaces and related measured points has been performed, the exercise can be extended to the reconstruction of the updated geometries on the measurement data.

5.2. Virtual Fitting

In the manufacturing of large-scale complex components, made by joining different sub-assemblies, is crucial to keep the process under control by evaluating the impact each manufacturing step is having on the geometrical compliance of the final product.

Efficiency can be improved if information embedded in measured data describing the real shape of parts are used for defining/guiding the alignment of pieces to be joined, and for implementing remedial actions during production to mitigate risk of product non-compliance.

Metrology has a key role in the manufacturing process, since it can help in the monitoring of the evolution of the parts towards the final configuration and in the evaluation of the best alignment in between the components in order to meet the dimensional requirements. In this context, methods such as Virtual Fitting (VF) or Virtual Assembly are common use.

Virtual Fitting is a technique which allows defining different alignments of objects by minimizing certain variables. By using measured data in describing the shape of objects, it is possible to define virtually the best relative position between imperfect parts that, for example, minimizes deviation from nominal (or out-of-tolerance) on the final product.

Spatial Analyzer (SA), which is the reference metrology software used in the ITER project, has been used as the reference software to build up the VF process in order to allow its full compatibility with most of the manufacturing process in which metrology is implemented. Thanks to the powerful SA best-fitting algorithm, it has been possible to manage optimization of huge amount of data (some thousands of points) in relative short time.
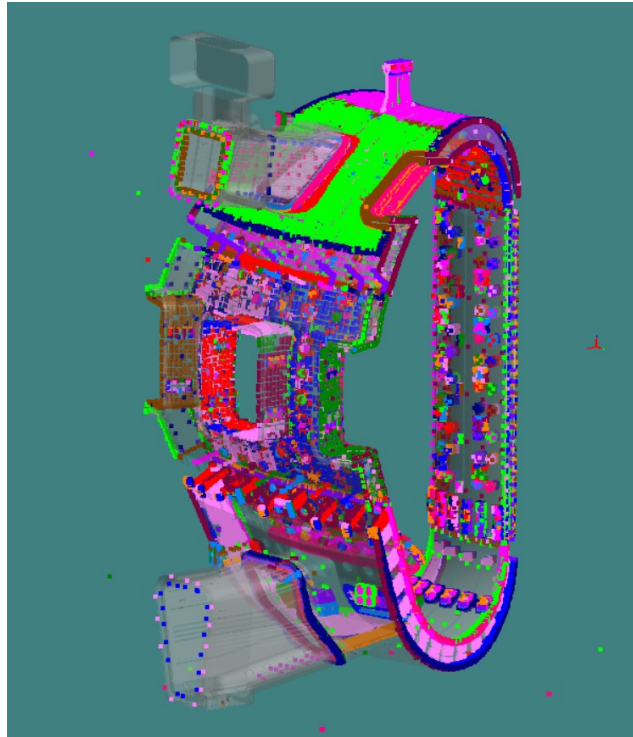
Figure 64: VV Sector 5 measured data

Linear least square optimization is the core of the tool. For a group of equally weighted measurements, the basic condition that is enforced in least squares adjustments is that the sum of the squares of the residuals is minimized. Residual is another term for the deviation between a measured value and the nominal model. For 3D coordinate metrology, one example of a residual would be the difference between the nominal XYZ coordinates for a point and the actual XYZ coordinates measurement. In this sense, rules mentioned above to be minimized must be intended as a set of residuals $e_{RMS,i}$ that should be minimized (each weighted specifically with the factor w_i if needed) when finding best relative position between parts. More precisely, the following functional is minimized:

$$E_{err}(w_i, e_{RMS,i}) = \sqrt{\sum_{i=1}^{N} w_i * e_{RMS,i}^2} \qquad (11)$$
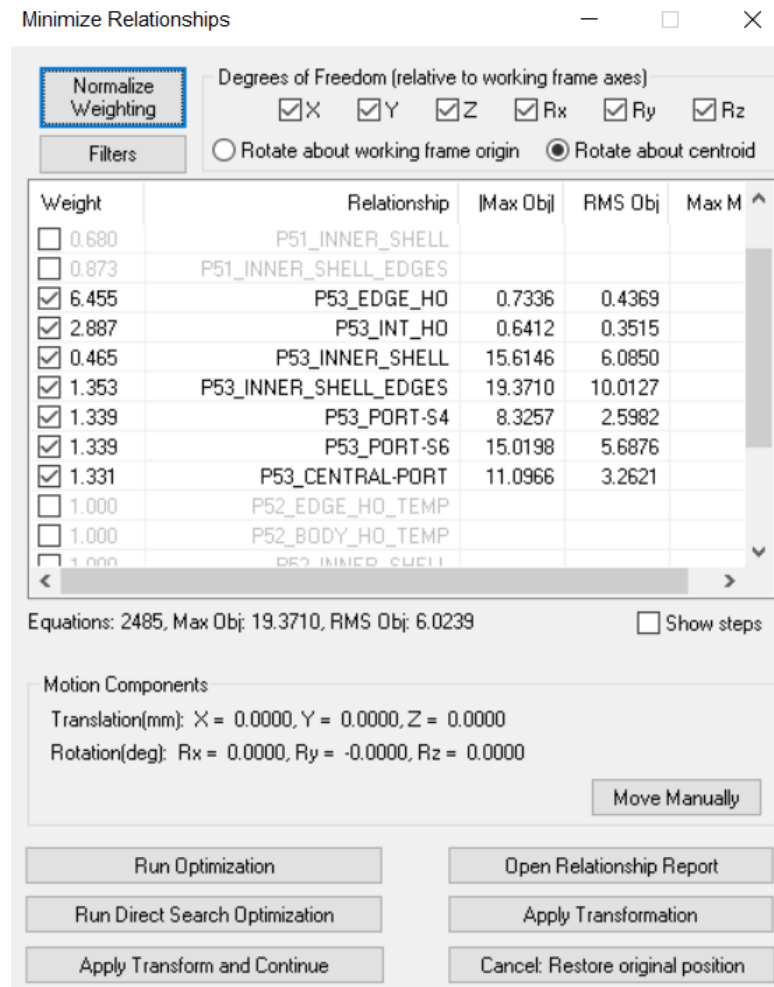
Figure 65: Example of residuals minimization algorithm interfaces

VF studies are based on the association of measured data describing the real shape of components to the nominal surface model, and on the minimization of resulting deviations. Also the collection of features belonging to different subcomponents can be used in the minimization, opening a new path in the optimization. The alignment can be driven not only by the minimization of measurements with respect to the nominal model, but it can be combined to the optimization of the non-ideal surface model representing the real shape. In other words, this set of rules can be defined to represent tolerance requirements certain features of the final product will have (note: tolerance requirements describe the maximum acceptable deviation/distance between a certain manufactured feature from nominal) or tolerance requirements certain interface of the parts should respect so they can be assembled.

In Figure 66 an example of definition of constraint between measurements and nominal model is shown, while in Figure 67, the tolerance requirements between real shape interfaces surfaces is shown.
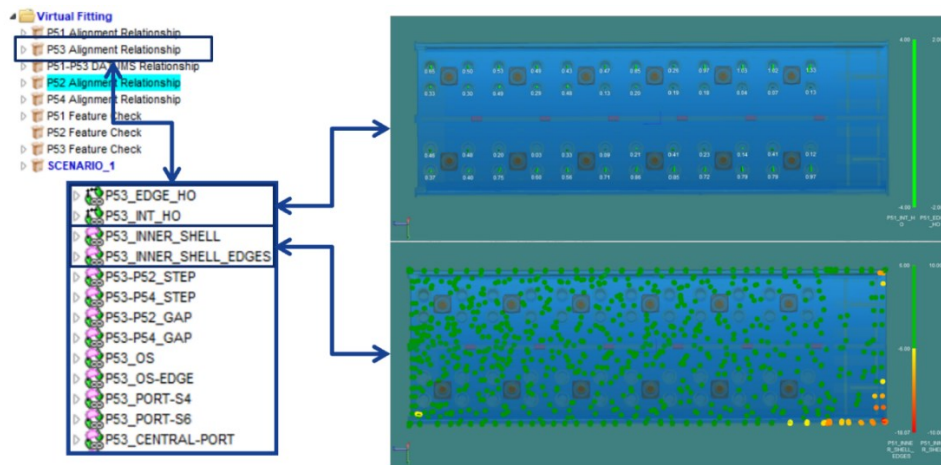
Figure 66: Relationships between nominal CAD and measured points
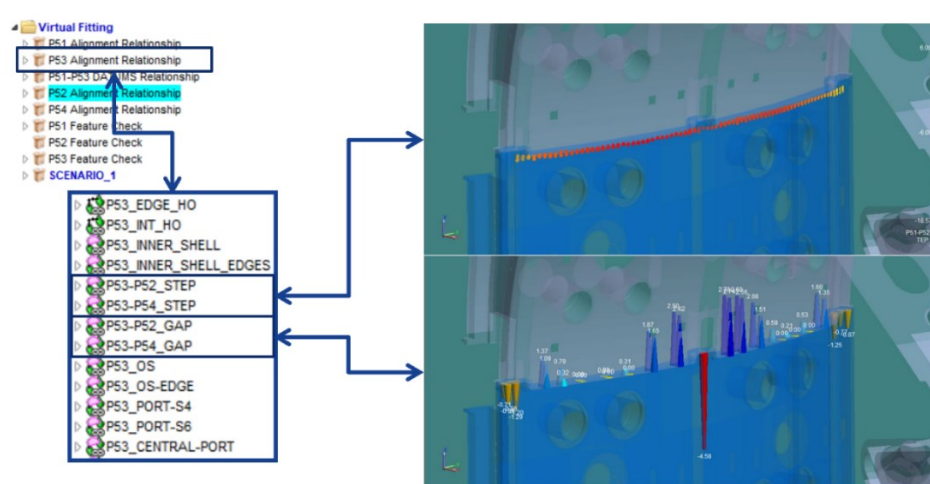
Figure 67: Relationships between reconstructed entities and measured points

With these techniques, the effect that geometrical imperfection, due to manufacturing processes, can have on the final product can be virtually evaluated and mitigated. Even if the obtained data must be considered an optimistic guess of the results, their correct usage results in an improvement of efficiency on time, cost and quality of the final product.

Applied to the Vacuum Vessel project, the main goal of the whole set of Virtual Fitting studies has been to predict and optimize the final position that features would have after the joining of the VV segments, keeping the requirement on weldability among them under control. In other words, Virtual Fitting studies allowed to find the best compromise between having the real pieces well-aligned to be welded and having under control the impact this alignment will have on the main geometrical requirements at the last stage of manufacturing. This information has proved to be crucial in order to define properly the final machining activities for finalizing DATUM features (mainly housings) at segment manufacturing stage.

This approach allowed to study different possible alignment scenarios resulting in different final shapes for the sector, to predict possible deviation from nominal and/or non-conformities the sector could have and to make them already known and assessed by the different stakeholders (including ITER IO) beforehand, in order to ease the final acceptance. For VV Sector 5 a set of 9 different scenarios has been studied.

Different rules were defined in order to keep under control the compliance of different features with final geometrical requirements (in terms of position and shape). Most important constraints were put on the final position of the axis of the housings, which define DATUM A and B, and the Inner Shell shape, defining the steps between adjacent segments to be welded. In addition, less relevant constraints on the final position and shape of Centring Keys and Intermodular Keys were considered, together with the final position of the VV interfaces with the ports, which need to be welded.

Up to date, the Virtual Fitting methodology has been used during the manufacturing of VV S5 and S4, driving the final machining strategy and alignment for the final welding of the four segments. Using this technique, the effort necessary to align huge and/or complex pieces has been significantly reduced, since the best relative position can be defined beforehand, virtually, performing VF studies. Furthermore, deviation the final product could have with respect to nominal has been foreseen before the assembly takes place and recovery actions discussed and agreed in advance to mitigate the risk of non-conformance on the final product.

Conclusions

In this work of thesis, an investigation on techniques and methods for the creation of a Digital Twin model has been performed.

The main two aspects on which the research has been focusing are the Association and reconstruction operation, as defined in 1.6 .

About the reconstruction exercises, a workflow has been developed in Ansys Workbench based on Radial Basis Function morphing and NURBS patching algorithms. As demonstrated in the TF WP and VV IS reconstructions, the procedure confirmed to guarantee high accuracy and flexibility in tackling geometrical reconstruction problems providing the capability to significantly reduce the effort if compared to a model reconstruction procedure adopting RE software.

Being linked to the initial CAD topology, the method is not suitable to as-built geometries in which deviation from the baseline configuration are related to the introduction of new features on the component (e.g. holes and pins). In the cases deviations due to the manufacturing process drive the CAD update, as in the big series production of components, the method offers short computational time and the possibility of automating the numerical process, making it a valuable alternative to commercial RE software.

In the association exercises, a Skin Surface model has been developed in Spatial Analyzer environment. The model, deployed in the TF project, is capable to assess automatically dimensional checks for seven variants of the ITER Toroidal Field coils. Related to the topic, the alignment of measurement data has also been investigated. Regarding this, the Virtual Fitting methodology has been deployed in the alignment of the VV segments. The evaluation of the deviation of the manufactured data from the nominal model and the relative position of the segment proved to be useful in finding the best compromise between weldability and final compliance of the component.

The research scope of this PhD set the basis for future development and integration of these operations in a common environment where the ITER Digital Twin can be built. Further manufacturing information related to processes not directly involving metrology can be included in the model. Other models, such as FEM, can be integrated in order to monitor the actual performances of the system during the several stages of its lifecycle.

Works cited

[1] "Wikipedia," [Online]. Available: https://en.wikipedia.org/wiki/Fourth_Industrial_Revolution.

[2] Uhlemann and al., "The Digital Twin: Realizing the Cyber-Physical Production System for Industry 4.0,," *Procedia CIRP,,* pp. Pages 335-340,, 2017,.

[3] Dantan and al., "Geometrical product specifications — model for product life cycle,," *Computer-Aided Design,,* Vols. Volume 40,, no. Issue 4,, pp. Pages 493-501,, 2008,.

[4] Geometrical product specifications (gps) – general concepts – part 1: Model for geometric specification and verification. ISO 17450-1., 2011.

[5] Schleich and al., "Skin Model Shapes: A new paradigm shift for geometric variations modelling in mechanical engineering,," *Computer-Aided Design,,* Vols. Volume 50,, pp. Pages 1-15,, 2014,.

[6] Wirtz, "Vectorial tolerancing: a basic element for quality control.," *Proceedings of the 3rd CIRP Seminar on Computer-Aided Tolerancing,* 1991.

[7]   Desrochers and al., "A dimensioning and tolerancing assistance model for cad/cam systems," *International Journal of Advanced Manufacturing Technology,* no. 9, pp. 352-361, 1994.

[8]   Chase and al., "Advanced Tolerancing Techniques," *John Wiley, Ch. Tolerance analysis of 2-D and 3-D mechanical assemblies with small kinematic adjustments,* 1997.

[9]   Davidson and al., "Using tolerance-maps to represent material condition on both a feature and a datum," *The 8th International CIRP Seminar on Computer Aided Tolerancing,* p. 92–101, 2003.

[10]   Giordano and al., "Tolerance analysis and synthesis by means of deviation domains, axi-symmetric cases," *Davidson, J. K. (Ed.), Models for Computer Aided Tolerancing in Design and Manufacturing,* p. 85–94, 2007.

[11]   Bourdet and al., "The concept of the small displacement torsor in metrology," *Advanced Mathematical Tools in Metrology II,* p. 110–122, 1996.

[12]   Hillyard and al., "Analysis of dimensions and tolerances in computer-aided mechanical design," *Comput Aided Design,* p. 161–166.

[13]   Requicha, "Representation of tolerances in solid modeling: issues and alternative approaches," *New York: Plenum Publishing Corporation Press,* p. 3–22, 1984.

[14]   Bourdet, "Contribution a la Mesure Tridimensionnelle: Modele d'ideentification des surfaces, Metrologie fonctionnelle des pieces

mecanniques, correction geometrique des machines a mesurer tridimentionnelles," *These d'Etat,* 1987.

[15] Jayaraman and al., "Geometric tolerancing I: virtual boundary requirement," *IBM J Res Dev,* vol. 33, no. 2, p. 90–104, 1989.

[16] Srinivasan and al., "Geometric tolerancing II: conditional tolerance," *IBM J Res Dev,* vol. 33, no. 2, p. 105–122, 1989.

[17] Etesami, "Mathematical model for geometric tolerances," *J Mech Design,* vol. 115, no. 2, p. 81–86, 1993.

[18] Shah and al., "Dimension and tolerance modeling and transformations in feature based design and manufacturing.," *J Intell Manuf,* vol. 9, no. 5, p. 475–488, 1998.

[19] Roy and al., "Information modelsfor Design Tolerancing: From Conceptual to the Detail Design," *ASME, DETC99 Conference,,* 1999.

[20] Ballu and al., "Discrete shape modeling for skin model representation," *Geometric Tolerancing of Products,* 2010.

[21] Ballu and al., "Univocal expression of functional and geometrical tolerances for design," *Proceedings of 4th CIRP seminar on Computer Aided Tolerancing,* 1995.

[22] V. Shapiro, "Solid modeling," *Tech. rep., University of Wisconsin,* 2001.

[23] Vajna and al., "CAx für Ingenieure.," *Springer Berlin Heidelberg,* 2009.

[24] "GUM Evaluation of measurement data — Guide to the expression of uncertainty in measurement," 1995.

[25] W. Les_Piegl, The_NURBS_Book.

[26] Biancolini and al., "A balanced load mapping method based on radial basis functions and fuzzy sets," *International Journal for Numerical Methods in Engineering,* vol. 115, no. 12, pp. 1411-1429, 2018.

[27] Groth and al., "RBF-based mesh morphing approach to perform icing simulations in the aviation sector," *Aircraft Engineering and Aerospace Technology,* vol. 91, no. 4, pp. 620-633, 2019.

[28] Biancolini and al., "Radial basis functions update of digital models on actual manufactured shapes," *Journal of Computational and Nonlinear Dynamics,* vol. 14, no. 2, 2019.

[29] Groth and al., "Fast high fidelity CFD/CSM fluid structure interaction using RBF mesh morphing and modal superposition method," *Aircraft Engineering and Aerospace Technology,* vol. 91, no. 6, pp. 893-904, 2019.

[30] Chiappa and al., "Post-processing of 2D FEM Q1 models for fracture mechanics by radial basis functions and balance equations," *International Journal of Mechanics,* vol. 13, 2019.

[31] Chiappa and al., "Improvement of 2D finite element analysis stress results by radial basis functions and balance equations," *International journal of mechanics,* vol. 13, 2019.

[32] Buhmann, "Radial Basis Functions: Theory and Implementations," *Cambridge Monographs on Applied and Computational Mathematics,* 2003.

[33] Fasshauer, "Meshfree Approximation Methods with Matlab," *Interdisciplinary Mathematical Sciences,* vol. 6, 2007.

[34] Biancolini, "Fast Radial Basis Functions for Engineering Applications," *Springer, Cham,* 2018.

[35] Davis, "Interpolation and Approximation," *Blaisdell Pub. Company,* 1963.

[36] Donné, "The European roadmap towards fusion electricity," *Philos. Trans. Roy. Soc. A,* vol. 377, no. 2141, p. 0432, 2017.

[37] Oliva and al., "Toward Completion and Delivery of the First EU ITER Magnets," *IEEE Transactions on Applied Superconductivity,* vol. 30, no. 4, pp. 1-13, 2020.

[38] Poncet and al., "EU ITER TF coil: Dimensional metrology, a key player in the double pancake integration," *Fusion Eng. Des.,* Vols. 98-99, p. 1135–1139, 2015.

[39] Jimenez and al., "Current centre line integration in the manufacturing process of the ITER toroidal field coils," *IEEE Trans. Appl. Supercond.,* vol. 30, no. 4, 2020.

[40] I. A. E. Agency, "ITER Technical Basis,," *ITER EDA Documentation Series,* vol. 24, 2002.

[41] Ioki and al., "Design and material selection for ITER first wall/blanket, divertor and vacuum vessel," *Journal of nuclear materials,* pp. 258-263, 1998.

[42] "RCC-MR. SECTION 1 - SUBSECTION Z, APPENDIX A16,," *afcen,,* 2007..

[43] "Memorandum_On_Virtual_Fitting__On_Line_Monitoring," vol. _2SXDBL_v1.

[44] Kim and al., "Manufacturing completion of the first ITER vacuum vessel sector," *Nuclear Fusion,* vol. 62, 2022.